



Dreiländertagung 2016

Gemeinsam mit dem
GEOSummit



Deutsche Gesellschaft für
Photogrammetrie,
Fernerkundung und
Geoinformation e.V.



Österreichische Gesellschaft
für Vermessung und
Geoinformation e.V.



Schweizerische Gesellschaft
für Photogrammetrie und
Fernerkundung

Dreiländertagung D-A-CH der DGPF, OVG und SGPF

36. Wissenschaftlich-Technische Jahrestagung

"Lösungen für eine Welt im Wandel"

Bern, 7. – 9. Juni 2016

Programm im Überblick

Dienstag, 7. Juni
ab 9:00 Uhr

11 Workshops
- Drohnen, 3D-Punktwolken,
BIM, etc.

16:30 Uhr
Mitgliederversammlung DGPF

ab 18:00 Uhr
Vorabend-Event
(Restaurant Grosse Schanze)

Mittwoch, 8. Juni
ab 9:00 Uhr

Eröffnungsveranstaltung
Plenarvortrag
33 Fachvorträge
Poster Session

Fachfirmen-Ausstellung
(GEOSummit-Messe)

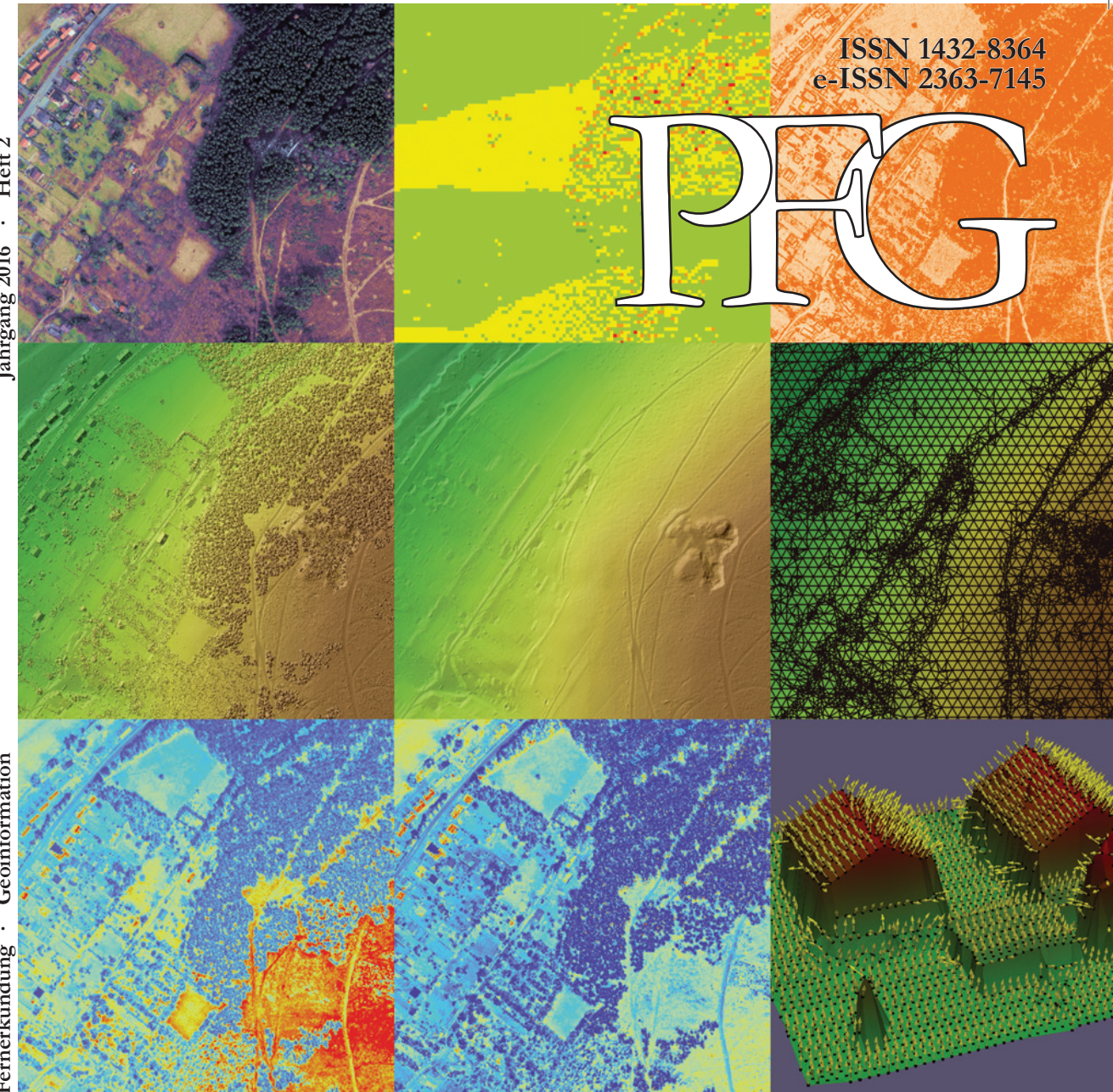
ab 18:00 Uhr
GEONight-Standparty mit
Preisverleihung

Donnerstag, 9. Juni
ab 9:00 Uhr

21 Fachvorträge
Fachfirmen-Ausstellung
(GEOSummit-Messe)

12:00 Uhr
Closing Session

14:30 Uhr
Ende der Tagung



ISSN 1432-8364
e-ISSN 2363-7145

PFG

Jahrgang 2016
Heft 2

Photogrammetrie Fernerkundung Geoinformation

Journal for Photogrammetry, Remote Sensing
and Geoinformation Science

Organ der Deutschen Gesellschaft für Photogrammetrie, Fernerkundung und Geoinformation (DGPF) e.V.
Indexed in Science Citation Index Expanded (SciSearch®)
Journal Citation Reports/Science Edition



Schweizerbart Science Publishers

Weitere Informationen unter www.dgpf.de oder www.sgpf.ch

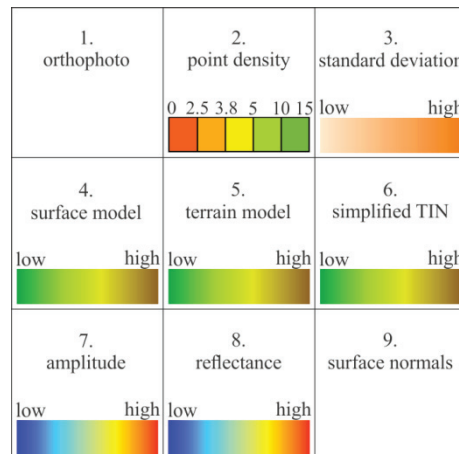
Anmeldung für Mitglieder unter www.geosummit.ch/DLT

Anmeldung für Nichtmitglieder unter www.geosummit.ch

Zum Titelbild

At the TU Wien (Department of Geodesy and Geoinformation) the scientific software OPALS (Orientation and Processing of Airborne Laser Scanning data) is being developed. The aim of this software is to provide a complete processing chain for airborne laser scanning data (waveform decomposition, georeferencing, quality control, structure line extraction, point cloud classification, DTM generation). OPALS was extensively used in our article comparing dense image matching and airborne laser scanning (ALS) for deriving terrain models.

The title image shows various results useful for analysing ALS data derived with different OPALS modules. The displayed results were computed based on ALS data of a study area discussed in the article. All sub images show the same area of interest (AOI) and are explained in the following.



1. The **orthophoto** is added as a visual guide.
2. The **point density** shows to which extent the ALS strips overlap within the AOI and is important for determining the geometric resolution of the models to be derived. Green indicates 5–10 points/m², yellow 3.8–5 points/m².
3. The **standard deviation** of the moving least squares interpolation used for deriving the surface model gives information about the local surface roughness.
4. The **surface model** is depicted using a superimposition of hill shading and hypsometric tinting.
5. The **terrain model** is depicted in the same way. Observe the emerging terrain features beneath the canopy.
6. From the high resolution surface model, a **simplified TIN** model obeying a maximum height tolerance and a maximum point distance can be derived. In contrast to areas with high curvature, e.g. break lines, the flat open terrain can be represented by only a few triangles.
7. For one of the strips covering the AOI a raster map of the returned signal **amplitude** (or intensity) is shown.
8. The surface **reflectance** can be derived for each 3D point from the signal amplitude using the sensor-to-object range and the incidence angle together with a few reference values. The reflectance is depicted using the same colour coding as the amplitude, clearly showing that the range dependent increase of the amplitude in the higher elevations is removed.
9. OPALS allows to derive the local **surface normals** for each 3D point using a certain set of neighbouring points. The derived normal vectors are here visualised using the open-source, data analysis and visualisation application ParaView.

For more information visit www.geo.tuwien.ac.at/opals

Dr. techn. CAMILLO RESSL, Technische Universität Wien, Department of Geodesy and Geoinformation, Gußhausstraße 27–29, A-1040 Vienna, Austria, e-mail: camillo.ressl@geo.tuwien.ac.at

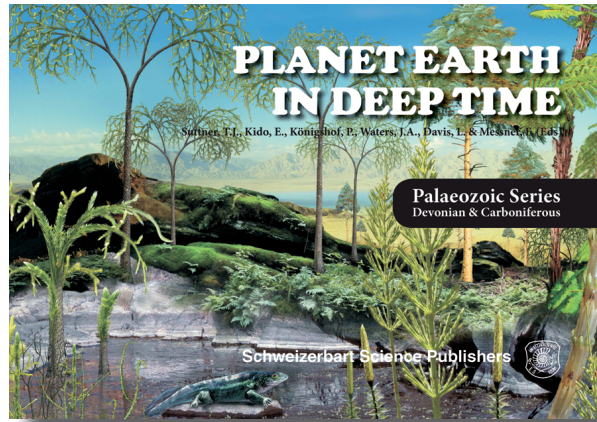
Dipl.-Ing. HERBERT BROCKMANN, Federal Institute of Hydrology, Department Geodesy, Am Mainzer Tor 1, D-56068 Koblenz, e-mail: brockmann@bafg.de

Dr. techn. GOTTFRIED MANDLBURGER, Technische Universität Wien, Department of Geodesy and Geoinformation, Gußhausstraße 27–29, A-1040 Vienna, Austria, e-mail: gottfried.mandlburger@geo.tuwien.ac.at

Prof. Dr. techn. NORBERT PFEIFER, Technische Universität Wien, Department of Geodesy and Geoinformation, Gußhausstraße 27–29, A-1040 Vienna, Austria, e-mail: norbert.pfeifer@geo.tuwien.ac.at



Record of climate change in Devonian and Carboniferous deposits around the world



Further information on this title:
www.schweizerbart.com/9783510653355

PLANET EARTH – IN DEEP TIME

Palaeozoic Series Devonian & Carboniferous

T.J. Suttner, E. Kido, P. Königshof, J.A. Waters, L. Davis, & F. Messner (Eds)

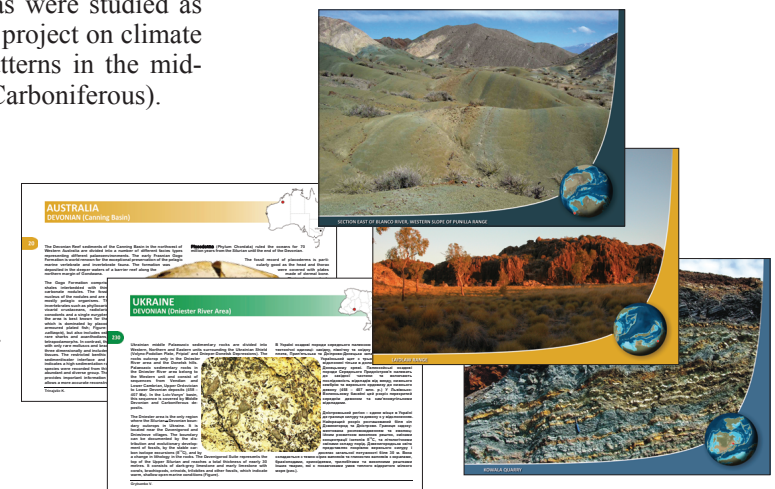
2016. X, 145 pages, 201 coloured figures, 30 x 21 cm, hardcover with dust cover

ISBN 978-3-510-65335-5 € 49.90



Each contribution describes (in English and the respective national language) the scope of the IGCP project in the respective country, exemplified by representative geological sections and/or regions there.

The authors intend to enhance the visibility and the perception of relevance of research on mid-Palaeozoic deposits beyond the Earth Science community.



Schweizerbart Science Publishers

Johannesstr. 3A, 70176 Stuttgart, Germany Tel. +49 (711) 351456-0 Fax. +49 (711) 351456-99
mail@schweizerbart.com

PFG

Photogrammetrie Fernerkundung Geoinformation

Journal for Photogrammetry, Remote Sensing
and Geoinformation Science

Organ der Deutschen Gesellschaft für Photogrammetrie,
Fernerkundung und Geoinformation (DGPF) e. V.

Jahrgang 2016, Heft 2

Herausgeber:
Prof. Dr.-Ing. Wolfgang Kresse

Schriftleiter:
Prof. Dr.-Ing. Stefan Hinz, Prof. Dr. techn. Franz Rottensteiner,
Prof. Dr. rer. nat. Christopher Conrad, Prof. Dr. rer. nat. Lars
Bernard und Dr.-Ing. Eckhardt Seyfert

Redaktionsbeirat (Editorial Board): Clement Atzberger, Andrew Frank,
Christian Heipke, Joachim Hill, Patrick Hostert, Hans-Gerd Maas, Wolfgang
Reinhardt, Camillo Ressl, Jochen Schiewe



E. Schweizerbart'sche Verlagsbuchhandlung
(Nägele u. Obermiller) Stuttgart 2016



Deutsche Gesellschaft für Photogrammetrie, Fernerkundung
und Geoinformation (DGPF) e.V.
Gegründet 1909

Die Deutsche Gesellschaft für Photogrammetrie, Fernerkundung und Geoinformation (DGPF) e.V. unterstützt als Mitglieds- bzw. Trägergesellschaft die folgenden Dachverbände:



International Society
for Photogrammetry
and Remote Sensing

DAGM

Deutsche Arbeits-
gemeinschaft für
Mustererkennung e.V.



GeoUnion
Alfred-Wegener-Stiftung

Herausgeber:

© 2016 Deutsche Gesellschaft für Photogrammetrie, Fernerkundung und Geoinformation (DGPF) e.V.
Präsident: Prof. Dr. Thomas Kolbe, Technische Universität München, Institut für Geodäsie, GIS und Landmanagement, Lehrstuhl für Geoinformatik, Arcisstraße 21, 80333 München, Germany, Tel. +49-89-289-23888
Geschäftsstelle: Tanja Nyc, c/o Technische Universität München, Institut für Geodäsie, GIS und Landmanagement, Lehrstuhl für Geoinformatik, Arcisstraße 21, 80333 München, Germany, Tel.: +49-89-289-22578, e-mail: geschaeftsstelle@dgpf.de

Published by: E. Schweizerbart'sche Verlagsbuchhandlung (Nägele u. Obermiller), Johannesstraße 3A, 70176 Stuttgart, Germany, Tel.: +49-711 351456-0, Fax: +49-711 351456-99, e-mail: mail@schweizerbart.de
Internet: <http://www.schweizerbart.de>

⊗ Gedruckt auf alterungsbeständigem Papier nach ISO 9706-1994

All rights reserved including translation into foreign languages. This journal or parts thereof may not be reproduced in any form without permission from the publishers.

Die Wiedergabe von Gebrauchsnamen, Handelsnamen, Warenbezeichnungen usw. in dieser Zeitschrift berechtigt auch ohne besondere Kennzeichnung nicht zu der Annahme, dass solche Namen im Sinne der Warenzeichen- und Markenschutz-Gesetzgebung als frei zu betrachten wären und daher von jedermann benutzt werden dürfen.

Verantwortlich für den Inhalt der Beiträge sind die Autoren.

ISSN 1432-8364 / e-ISSN 2363-7145

Science Citation Index Expanded (also known as SciSearch®) Journal Citation Reports/Science Edition
Hauptgeschäftsführer: Prof. Dr.-Ing. Wolfgang Kresse, Hochschule Neubrandenburg, Fachbereich Landschaftswissenschaften und Geomatik, Brodaer Straße 2, 17033 Neubrandenburg, Germany, e-mail: kresse@hs-nb.de
Schriftleiter: Prof. Dr.-Ing. Stefan Hinz, Karlsruher Institut für Technologie – KIT, Institut für Photogrammetrie und Fernerkundung, Englerstraße 7, 76131 Karlsruhe, Germany, e-mail: stefan.hinz@ipf.uni-karlsruhe.de, Prof. Dr. techn. Franz Rottensteiner, Leibniz Universität Hannover, Institut für Photogrammetrie und Geoinformation, Nienburger Straße 1, 30167 Hannover, Germany, e-mail: rottenstein@ipi.uni-hannover.de, Prof. Dr. rer. nat. Christopher Conrad, Universität Würzburg, Institut für Geographie und Geologie, Oswald-Külpe-Weg 86, 97074 Würzburg, Germany, e-mail: christopher.conrad@uni-wuerzburg.de, Prof. Dr. rer. nat. Lars Bernard, Technische Universität Dresden, Fachrichtung Geowissenschaften, Helmholtzstraße 10, 01062 Dresden, Germany, e-mail: lars.bernard@tu-dresden.de, und Dr.-Ing. Eckhardt Seyfert, Landesvermessung und Geobasisinformation Brandenburg, Heinrich-Mann-Allee 103, 14473 Potsdam, Germany, e-mail: eckhardt.seyfert@geobasis-bb.de

Erscheinungsweise: 6 Hefte pro Jahrgang.

Bezugspreis im Abonnement: € 262,- pro Jahrgang. Mitglieder der DGPF erhalten die Zeitschrift kostenlos.
Der Online-Zugang ist im regulären Subskriptionspreis enthalten.

Anzeigenverwaltung: E. Schweizerbart'sche Verlagsbuchhandlung (Nägele u. Obermiller), Johannesstraße 3A, 70176 Stuttgart, Germany, Tel.: +49-711 351456-0; Fax: +49-711 351456-99.

e-mail: mail@schweizerbart.de, Internet: <http://www.schweizerbart.de>

Bernhard Harzer Verlag GmbH, Westmarkstraße 59/59a, 76227 Karlsruhe, Germany, Tel.: +49-721 944020, Fax: +49-721 9440230, e-mail: Info@harzer.de, Internet: www.harzer.de

Printed in Germany by Tutte Druckerei & Verlagsservice GmbH, 94121 Salzwedel, Germany.

PFG – Jahrgang 2016, Heft 2

Inhaltsverzeichnis

Originalbeiträge

RESSL, C., BROCMANN, H., MANDLBURGER, G. & PFEIFER, N.: Dense Image Matching vs. Airborne Laser Scanning – Comparison of two methods for deriving terrain models	57
KAASALAINEN, S., NEVALAINEN, O., HAKALA, T. & ANTTILA, K.: Incidence Angle Dependency of Leaf Vegetation Indices from Hyperspectral Lidar Measurements	75
BARETH, G., BENDING, J., TILLY, N., HOFFMEISTER, D., AASEN, H. & BOLTEN, A.: A Comparison of UAV- and TLS-derived Plant Height for Crop Monitoring: Using Polygon Grids for the Analysis of Crop Surface Models (CSMs)	85

Mitteilungen

Berichte von Veranstaltungen	
ISPRS Geospatial Week 2015, 28. September – 2. Oktober 2015, La Grande Motte, Frankreich	95
Tagung „Alle Orte, alle Zeiten“, 4. und 5. November 2015, Hamburg	96
Persönliches	
Nachruf auf Kennert Torlegård	99
Hochschulnachrichten	
Karlsruher Institut für Technologie, Dissertation Clémence Dubois	100
Neuerscheinung	101
Veranstaltungskalender	102
Korporative Mitglieder	103

Zusammenfassungen der „Originalbeiträge“ und der „Beiträge aus Wissenschaft und Praxis“
(deutsch und englisch) sind auch verfügbar unter www.dgpf.de/neu/pfg/ausgaben.htm



Dense Image Matching vs. Airborne Laser Scanning – Comparison of two methods for deriving terrain models

CAMILLO RESSL, Vienna, Austria, HERBERT BROCKMANN, Koblenz,
GOTTFRIED MANDLBURGER & NORBERT PFEIFER, Vienna, Austria

Keywords: laser scanning, image matching, terrain, accuracy

Summary: In this article the performance of dense image matching (DIM) is investigated regarding its capability to yield terrain data, especially close to free-flowing water ways. Therefore, over two study areas aerial images with ground sampling distances 10 cm and 6 cm, respectively, are used for matching with the software packages Match-T (Trimble) and SURE (nframes). The matching results over areas with varying vegetation density (open grassland, loose and dense vegetation) are then compared with ALS reference data. Two parameters are investigated: (a) the terrain coverage; i.e. the percentage of the terrain covered by the matching results; and (b) the height accuracy of the matching results in the terrain class. The results show that DIM can only deliver terrain data in areas with no or very loose vegetation. Additionally, it was found that in the case of open grassland the DIM terrain heights were systematically higher by 10 cm compared with the ALS terrain heights. This is caused by the fact that ALS can penetrate the vegetation to some extent whereas matching occurs on top of the grass. The very good height accuracy (as standard deviation) obtainable by DIM, which is only slightly worse than the ALS accuracy (6.5 cm vs. 4.5 cm), is encouraging. Motivated by these results new possible applications arise for the respective authorities (the German Federal Institute of Hydrology and the German Federal Water and Shipping Administration), e.g. capturing dry fallen areas of free flowing rivers during documentation at low water levels.

Zusammenfassung: Vergleich von Bild-Matching und Laserscanning zur Ableitung von Geländemodellen. In diesem Aufsatz wird untersucht, in wie weit das Matching von digitalen Bildern für die Ableitung von digitalen Geländemodellen speziell im Bereich von freifließenden Bundeswasserstraßen verwendet werden kann. Dafür wird für Luftbilder über zwei Untersuchungsgebieten (Bodenpixelgröße 10 cm bzw. 6 cm) ein Matching mit zwei kommerziellen Programmen (Match-T (Trimble) und SURE (nframes)) durchgeführt. Die sich ergebenden Matching-Ergebnisse werden in Bereichen mit unterschiedlicher Vegetationsdichte (offene Wiese, lockere und dichte Vegetation) mit Laserscanning-Referenzdaten verglichen. Zwei Parameter werden dabei untersucht: (a) die Geländeabdeckung, d. h. der Prozentsatz der Geländeoberfläche, der durch die Matching-Ergebnisse abgedeckt wird; und (b) die Höhengenauigkeit der Matching-Ergebnisse in der Gelände-Klasse. Die Ergebnisse zeigen, dass per Bild-Matching Geländehöhen nur in Bereichen mit keiner oder nur lockerer Vegetation bestimmt werden können. Zusätzlich hat sich gezeigt, dass auf offenen Wiesen die Matching-Höhen systematisch um 10 cm höher als die ALS-Höhen liegen. Das ist eine Folge davon, dass das Lasersignal die Vegetation durch Lücken im Blattwerk zu einem gewissen Teil durchdringen während das Matching nur an den Gras spitzen erfolgen kann. Bemerkenswert ist die sehr gute Höhengenauigkeit (gemessen als Standardabweichung), die mithilfe von Bild-Matching erreicht werden kann. Sie ist mit 6.5 cm nur geringfügig schlechter als die ALS-Genauigkeit von 4.5 cm. Für die verantwortlichen Behörden (Bundesanstalt für Gewässerkunde, sowie Wasser- und Schifffahrtsverwaltung des Bundes) zeigen diese Ergebnisse neue mögliche Anwendungen auf, z.B. die Erfassung von trocken gefallenen Bereichen an Fließgewässern im Rahmen von Niedrigwasserdokumentationen.

1 Introduction

Over the past 15 years airborne laser scanning (ALS) was generally preferred over stereo photogrammetry for acquiring data for digital terrain models. This is primarily caused by the ability of ALS to penetrate vegetation and yield measurements on the ground (BALTSAVIAS 1999, PETZOLD et al. 1999).

The same time span, however, showed also two major advancements in photogrammetry: a) the development of digital aerial cameras (LEBERL et al. 2012), which allow a complete digital workflow, very high image forward overlaps and small ground sampling distances (GSD), and b) the development of dense image matching techniques (DIM), which enable the automatic generation of dense 3D point clouds from overlapping images with a resolution close to the GSD (HIRSCHMÜLLER 2008).

Many articles have been published on the DIM-based derivation of digital surface models (DSMs) and their quality evaluation using ALS reference data, e.g. VASTARANTA et al. (2013), HAALA & ROTHERMEL (2012), XIAO et al. (2012), HAALA et al. (2010). However, the usage of DIM for digital terrain models (DTM) has not been investigated much - especially not in vegetated areas. In BAUERHANSL et al. (2004) vegetation was considered but only sparse matching was applied to scanned analogue images, leading to unsatisfying results in wooded areas.

Motivated by the mentioned advancements in photogrammetry the German Federal Institute of Hydrology (Bundesanstalt für Gewässerkunde, BfG) in cooperation with the German Federal Water and Shipping Administration (Wasser- und Schifffahrtsverwaltung des Bundes, WSV) and the Department of Geodesy and Geoinformation, TU Wien, initiated a pilot project to investigate the practical performance of DIM for the derivation of a DTM-W (digital terrain model of watercourses). The DTM-W is an important dataset in particular for addressing hydraulic and hydrological issues. It represents the ground of the flow-effective riparian area of a waterway as well as the riverbed with a typical resolution of $1\text{ m} \times 1\text{ m}$. The main objective of this project was to clarify whether DIM can be used as a cost-effective alternative to ALS

for data collection with at least 4 points per m^2 for processing and updating the DTM-W of the forelands and the dry fallen parts of the littoral zone (during low water situations).

This article presents the main technical outcomes of these investigations. First a brief description of ALS and DIM is given in section 2. The results obtained at two representative study areas (Weser/Bad Karlshafen and Elbe/Klöden) are presented in sections 3 and 4 using profiles, ground coverage and height accuracy. Finally, section 5 draws the main conclusions.

2 Methods of Data Acquisition

2.1 Airborne Laserscanning (ALS)

ALS applies an active polar multi-sensor system (WEHR & LOHR 1999, SHAN & TOTH 2008). A scanner is mounted on a flying platform and emits usually infrared laser pulses. Each pulse interacts with various objects along its path, e.g. leafs, twigs, bushes and ground. Each of these illuminated objects scatters the emitted pulse to some extent, causing a part of it to return as echo to the detector of the scanner. The respective time of flight allows to determine the distance between the scanner and each object. The 3D coordinates of these objects result from the polar scanner measurements (deflection angle and range) and the position and rotation of the sensors (measured using a global navigation satellite system (GNSS) and an inertial navigation system). Consequently, a single sight to an object point is sufficient to determine that point's 3D coordinates. Therefore, the gaps in the canopy, through which points on the ground are measured, can be quite small.

2.2 Dense Image Matching (DIM)

Image matching is based on the photogrammetric reconstruction principle. In this case, each object point must be visible in at least two images. Each image point and the respective projection centre define a viewing ray. Provided the interior orientation (principal distance, principal point, lens distortion) and the exterior orientation (spatial location and rotation of the image) are known, the coordinates of the object point can be reconstructed using the spatial intersection of the viewing rays.

Nowadays the term *matching* is often used for the whole process of image point extraction, searching for corresponding points in overlapping images and spatial intersection. Matching, originally, just referred to the 2nd step (VOSSELMAN et al. 2004): the automatic search for correspondences (in two images). The classical approaches were feature based matching (FBM) and area based matching (ABM). Both approaches are *local* in the sense that each correspondence is found independently of already established correspondences in the neighbourhood. In the case of ABM an additional locality is introduced because a small correlation window is used, which inherently assumes that all pixels in that window stem from object points at the same depth. This assumption is clearly not valid e.g. in the case of depth discontinuities and occlusions. These classical approaches are *sparse* in the sense that only a small fraction of the pixels in each image generates 3D points.

In contrast to this, *dense image matching* (DIM) tries to find correspondences for every n-th pixel. For n=1 the resulting 3D point cloud will have a point distance identical to the GSD of the images. Nowadays the GSD of aerial images is typically in the range of 5 cm–20 cm.

In recent years semi-global matching (SGM) was introduced (HIRSCHMÜLLER 2008) and disseminated (ROTHERMEL et al. 2012). For SGM, first, the colour values of the pixels are transformed into a more robust domain, e.g. using census transformation (ZABIH & WOODFILL 1994). Afterwards SGM performs dense image matching for every pixel by minimising the difference of the transformed values of the pixel in the left and the corresponding pixel in the right image. In order to improve the robustness of this approach and to bridge areas of poor texture SGM applies a smoothness constraint, which favours correspondences that produce neighbouring points having the same depth. Both, the difference of the transformed pixel values and the smoothness constraint, are combined in a weighted sum. This sum is then minimised as an energy function. Depending on these weights the smoothness constraint may be violated in case of depth changes, e.g. at roofs or tilted planes, because there, the pixel value difference can be dramatically reduced for non-neighbouring pixels.

Because two image rays to an object point are required to determine that point's 3D coordinates, matching images of vegetated areas will primarily deliver points on the visible top of the canopy. Matching points on the ground through gaps in the canopy is difficult for two reasons: (i) generally, it is not very likely that the same point on the ground will be visible through the canopy in images made from two different projection centres, (ii) even if this happened, dark shadows on the forest floor might cause bad image texture. Consequently, at such locations matching is prevented at all or the smoothness constraint takes over and keeps the heights at the dominant visible object (the canopy). However, with increasing size of the gaps and decreasing density of the vegetation, chances will grow that matching can deliver points on the ground.

2.3 Used Matching Software

In this study the following two commercially available software packages were used: nframes SURE (version 20140716_2245) and Trimble Match-T (version 5.5). Both apply an SGM-based approach (ROTHERMEL et al. 2012 and TRIMBLE 2014).

2.3.1 SURE

SURE uses each image as so-called *base image*. The software matches every pixel in this base image with pixels from each directly neighbouring image (of the same strip and the neighbouring strips) and then computes a multi-image-based spatial intersection. At the end the point clouds obtained for each base image are merged by a median-based fusion to form a grid of the entire project area. In this way the high image overlaps are exploited very well. SURE offers a scenario parameter which defines the actual matching parameters, controlling e.g. the applied census transformation, the considered disparity ranges, and the selected image pairs based on acceptable viewing angles. The following scenario settings were tested: DEFAULT, AERIAL8080 and OBLIQUE.

2.3.2 Match-T

Match-T uses an SGM implementation which internally is termed *cost based matching* (CBM). The resulting point cloud, however, is not the set of points that were originally computed by spatial intersection but an interpolated grid, with a grid spacing that defaults to three times the GSD. In the version 5.4, calling Match-T with all images of a block worked in the following way: Based on the forward and cross overlaps of the images a certain structure of regions is established. Each region is covered by a single pair of consecutive images, whose matching results are solely responsible for the heights in that particular region. In this way each height in the final model of the entire project area is eventually derived from two images only. The possibly very large image overlaps are not exploited (e.g. at 80 % forward overlap each object point is mapped into five images). Additionally, all matched points have practically the same height accuracy – the one stemming from the image pair with the smallest base.

Therefore, in the version 5.5 a new option called *UAS* was included, which better exploits high image overlaps that typically occur with images from unmanned aerial systems. However, the manual of Match-T does not explain how this UAS method actually works.

Alternatively this limited exploitation of high image overlaps can also be avoided by user interaction. We implemented a workflow by calling Match-T in a batch mode where each matching job consists of only two images and the set of all jobs comprises all possible image pairs (within a selected range of image overlaps). In the end all pair-wise grid results are fused by computing the median of all heights per grid cell. In case of a flight with 80 % forward overlap each object point is mapped into five images and thus is contained in four image pairs with 80 % overlap. If the strips were flown with 50 % cross overlap each point appears in two strips. Then in total each point is contained in eight image pairs and during the fusion the median of eight heights is computed. In sections 3 and 4 the used range of image overlaps for this fusion method will be encoded in the name of the Match-T results; e.g. (85705570 q) means that the result was derived using all image pairs

in the same strip with overlaps 85 %, 70 % and 55 %, as well as image pairs covering two strips with overlap 70 %.

2.4 Study Areas

ALS and image data were available for two project regions in Germany. In each region a small study area with a varying vegetation density was selected.

Over project region **Weser/Bad Karlshafen** (total area 565 km²) the images were acquired using a Zeiss DMC-II (GSD: 10 cm, forward overlap: 85 %, cross overlap: 70 %, PAN+RGB, date: April 2013). The laser data were acquired using a Riegl LMS-Q 560 (point density: 6 points/m², date: March 2011). Both flights occurred in early spring before foliation. The selected study area, see Fig. 1, has a size of 1500 m × 1500 m and is covered by 91 images. This area is of interest for three reasons: (i) heterogeneous land cover (high, low, dense and loose vegetation, settlement, water), (ii) rough and smooth surface, (iii) flight parameters (very high overlap and medium sized GSD). DIM grids were generated from the PAN images using SURE with a grid width of 10 cm. The Match-T products were generated with a grid width of 25 cm. The SURE grid is visualised in Fig. 3a.

Over project region **Elbe/Klöden** (total area 34 km²) the images were acquired using a Vexcel UltraCam X (GSD: 6 cm, forward overlap: 80 %, cross overlap: 70 %, PAN+RGB(I), date: April 2013). The laser data were acquired simultaneously using an Optech ALTM Gemini (point density: 4 points/m²). The flight occurred in early spring before foliation. The selected study area, see Fig. 2, has a size of 1000 m × 1000 m and is covered by 98 images. This area is of interest for three reasons: (i) smooth and homogenous coverage (grassland), (ii) simultaneous image and laser acquisition, (iii) flight parameters (very high overlap and small GSD). Note that the ALS data do not fully cover the study area; this is later considered by a mask. DIM grids generated from the PAN images using SURE have a grid width of 7 cm, the ones using Match-T have a grid width of 15 cm. The SURE grid is visualised in Fig. 3b.

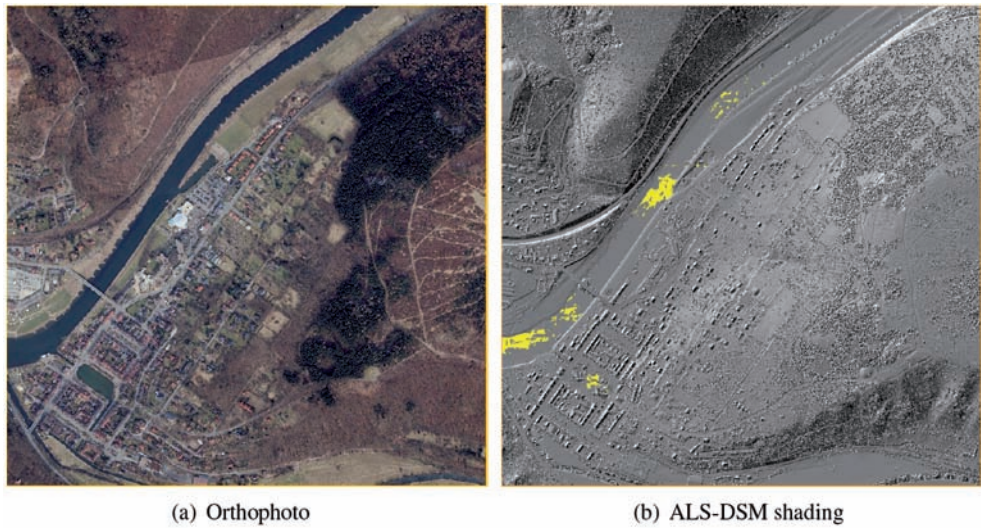


Fig. 1: The selected study area Weser/Bad Karlshafen. East-west extension 1500 m. Yellow = no data. The ALS-DSM used only the last echoes. For the orthophoto-mosaic no colour correction was applied.

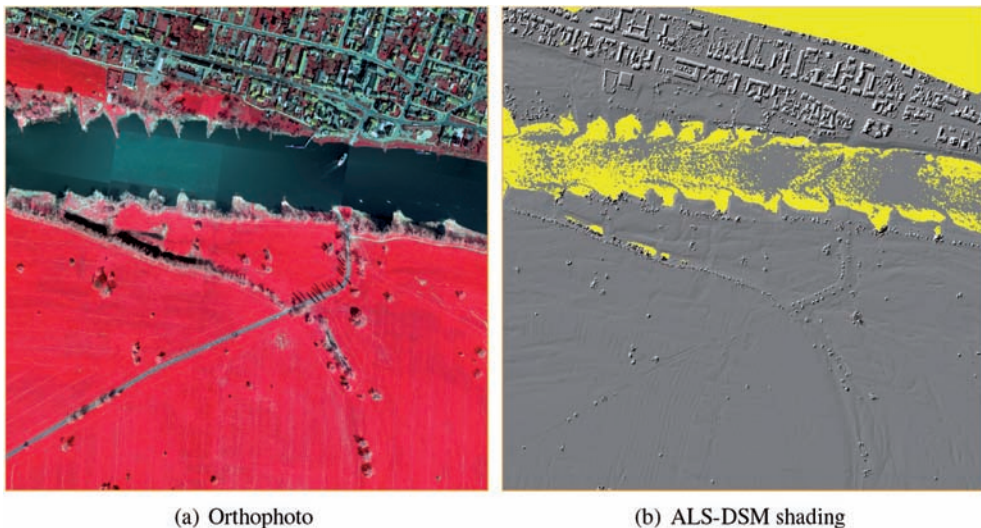


Fig. 2: The selected study area Elbe/Klöden. East-west extension 1000 m. Yellow = no data. The ALS-DSM used only the last echoes. For the orthophoto-mosaic the false-colour composite images were used and no colour correction was applied.

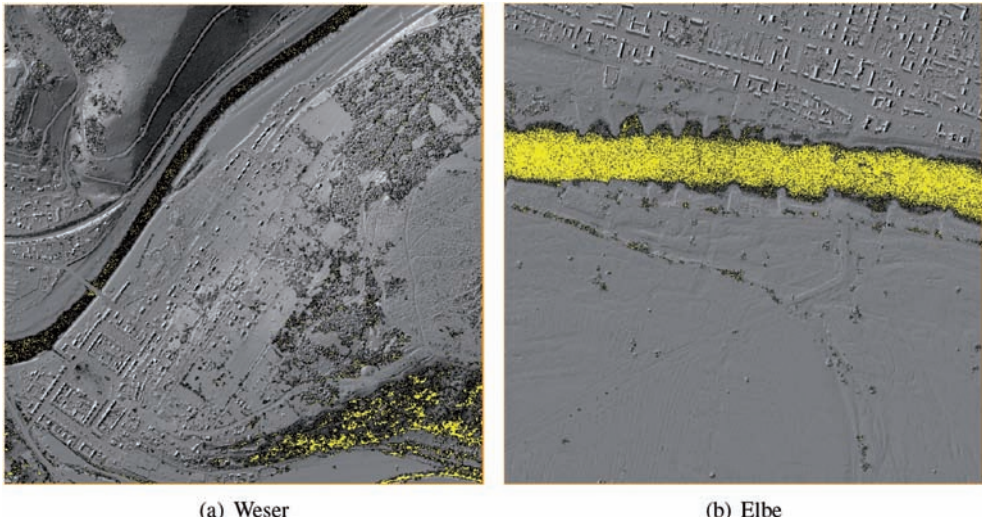


Fig. 3: Shadings of the SURE grids in study area Weser (left) and Elbe (right). Yellow = no data. Note that in water areas DIM either delivers wrong heights or no data at all.

For both project regions the ALS data were acquired in accordance with the guideline of the public mapping authorities (AdV 2013). These guidelines prescribe that at least 95 % of the height differences between ALS and check points should be smaller than 15 cm in flat to undulating terrain and smaller than 30 cm in steeper areas distributed over all land cover classes. The accuracy of the ALS-DTMs in the two study areas does not only conform with these specifications, it actually surpasses them – as it is documented using reference data. For the DTM-W over the project region Weser with 565 km^2 5170 check points were measured and 99 % of their differences meet the above mentioned specifications. For the project region of Elbe with 34 km^2 22210 check points were used and 97 % fulfil the requirements mentioned above.

For both project regions the images were oriented using the standard procedure of GNSS assisted aerial triangulation, during which automatic tie points were extracted with an accuracy of 0.1 pixel. Depending on their multiplicity the estimated height accuracy of the tie points ranges from 2 cm to 11 cm (Weser) and 1 cm to 5 cm (Elbe).

In section 3 the applied methods and results are presented for study area Weser. The same

methods are applied in study area Elbe in section 4, where only the results are presented.

3 Applied Methods and Results for Study Area Weser

The analysis of the matching results is done qualitatively using profiles and quantitatively by considering two parameters: (a) the **terrain coverage**; i.e. the percentage of the terrain covered by the matching results; and (b) the **height accuracy** of the matching results in the terrain class. The reference for both parameters is the DTM derived from the ALS data.

3.1 Profiles

Fig. 4a shows a profile through *dense vegetation*. ALS delivers echoes from the top of the trees, within the vegetation and from the ground. As mentioned at the end of section 2.2, DIM only delivers points at the top of the trees in the vegetated parts. Only in clearings DIM can deliver points on the ground.

Fig. 4b shows a profile through *loose vegetation*. Again ALS delivers echoes from the top of the trees, within the vegetation and from the ground. However, DIM practically only delivers points on the ground. Obviously, the gaps

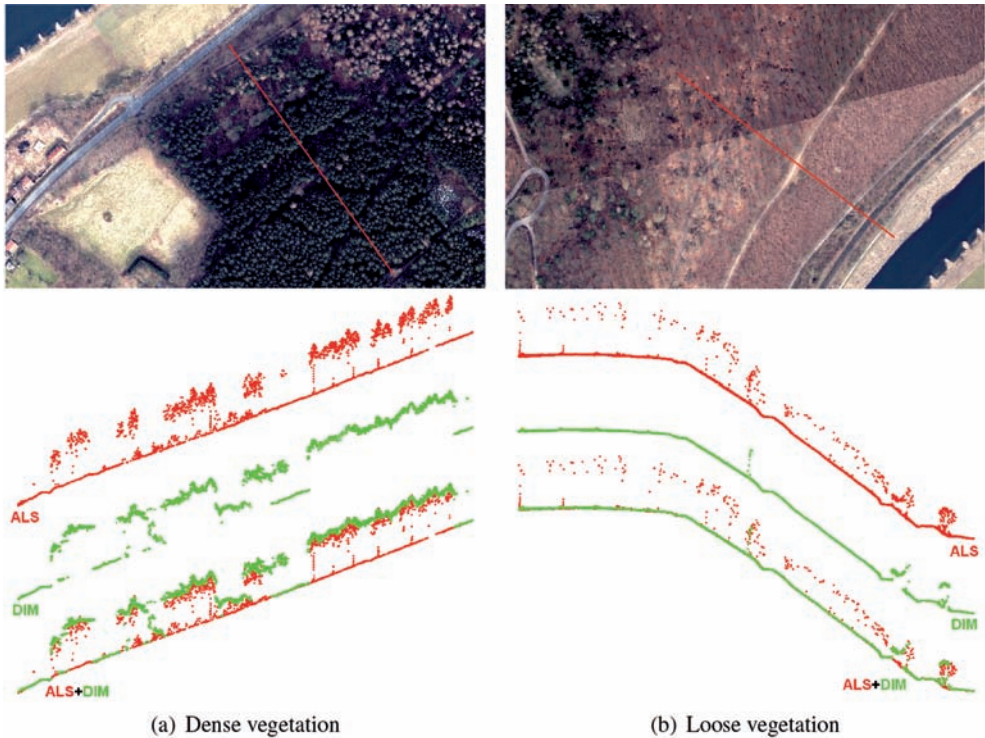


Fig. 4: Two profiles in study area Weser. The ALS points are shown in red, the DIM points (from SURE (OBLIQUE)) in green. In the last row the DIM points are superimposed on the ALS points. The east west extension of both orthophoto sections is about 500 m. The vertical direction of the profiles is magnified by a factor of 1.5.

in the vegetation are wide enough and thanks to the smoothness constraint, DIM is not disturbed by the loosely distributed trees with no or only little foliage.

3.2 Classification of Terrain Points

As shown in the previous section, the success rate of DIM for delivering points on the ground is influenced by the density of the vegetation. Therefore, the ALS-DTM is used as the reference for the subsequent classification of individual points into terrain and off-terrain points. This DTM is derived from the given ALS data using all last echoes by means of robust interpolation (KRAUS & PFEIFER 1998) with a grid width of 0.5 m. The DTM was visually analysed using a shaded relief map to ensure that it is free of gross errors.

The classification of ALS and DIM points into terrain points and off-terrain points is

performed using their distance ΔZ to the ALS-DTM.

3.2.1 ALS Classification

Fig. 5 shows the histogram of the differences ΔZ of the last echos to their DTM in study area Weser – limited to the interval $\text{abs}(\Delta Z) < 20 \text{ cm}$. The ordinary standard deviation $\sigma_{\Delta Z}$ of these differences is 4.7 cm. The histogram is very similar to a Gaussian distribution with zero mean. Based on that distribution the robust standard deviation σ_{MAD} is 3.0 cm¹. The difference between these two dispersion values shows that bigger differences occur slightly

¹ σ_{MAD} is a robust estimator for the standard deviation of a Gaussian distribution derived as $\sigma_{MAD} = 1.4826 \cdot MAD$; where MAD is the median of absolute differences (with respect to the median) derived from all values.

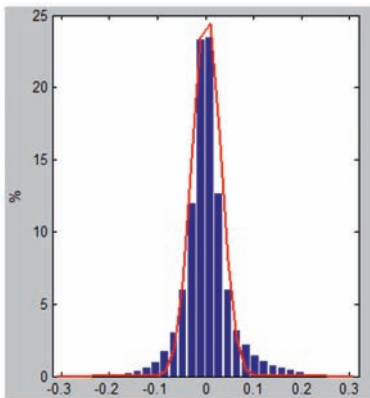


Fig. 5: Histogram of the height differences ΔZ (in m) of the last echos to the ALS-DTM in study area Weser; limited to $\text{abs}(\Delta Z) < 20 \text{ cm}$. A Gaussian distribution with zero expectation and standard deviation 4 cm is drawn in red.

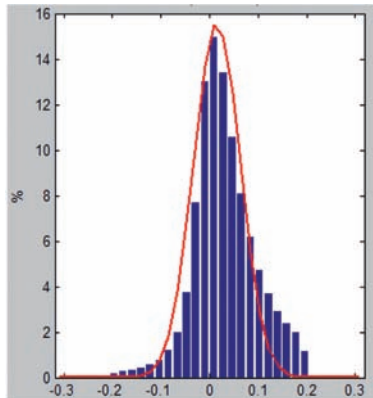


Fig. 6: Histogram of the height differences ΔZ (in m) of the SURE grid (OBLIQUE) to the ALS-DTM in study area Weser; limited to $\text{abs}(\Delta Z) < 20 \text{ cm}$. A Gaussian distribution with expectation 1.5 cm and standard deviation 4.8 cm is drawn in red.

more often than one would expect from a Gaussian distribution. This is a phenomenon that often occurs with real data. It can be explained by the mixture of ΔZ groups with different dispersions. ΔZ values in smooth areas (streets, parking lots) will have very small standard deviations, whereas ΔZ values in rough areas (forest floor) will have bigger standard deviations. The mean is always zero, thus the mixture of these different ΔZ groups will produce a mono-modal distribution with a steeper peak.

All last echoes with $\text{abs}(\Delta Z) < \Delta Z_{\max}$, for a certain threshold ΔZ_{\max} , are classified as terrain. Because the histogram is very similar to a Gaussian distribution we adopt the three-sigma-rule, which is thus fulfilled by $> 99\%$ of the terrain points; i.e. it is very unlikely that a terrain point has a ΔZ larger than this threshold. We use the value $\Delta Z_{\max} = 3 \cdot \sigma_{\Delta Z} \approx 15 \text{ cm}$. In order to evaluate the effect of this choice on the quantitative results, we apply also the ΔZ_{\max} values 10 cm (based on three times σ_{MAD}) and 20 cm (the whole range considered for the histogram).

3.2.2 DIM Classification

The DIM points are classified also by their height differences ΔZ with respect to the ALS-DTM. Fig. 6 shows the ΔZ histogram

for the result of SURE (OBLIQUE) limited to $\text{abs}(\Delta Z) < 20 \text{ cm}$. All DIM variants produce histograms similar to that figure. The negative side of that histogram shows a Gaussian-like shape which therefore justifies cutting off the histogram at 20 cm. As a visual aid the figure also displays a Gaussian distribution with 1.5 cm expectation and a standard deviation of 4.8 cm. It is clearly visible that the histogram is skewed towards the right. This is primarily caused by matching errors that appear as small transitions at height discontinuities (e.g. at cars; see Fig. 7).

In study area Weser the image flight occurred two years later than the ALS flight. In order to compensate for possible terrain changes the following actions were taken. Negative terrain changes like excavations are considered by adapting the classification interval to $[-150, 20] \text{ cm}$ for the entire area. All DIM points within this interval are classified as terrain. Positive terrain changes, e.g. mounds, can not be considered by enlarging the classification interval to the positive side, because then also many off-terrain points would be classified as terrain. To consider the positive terrain changes, a mask was manually digitized that excludes these parts of the study area from the investigation. Additionally, this mask considers all locations at which DIM can not measure the

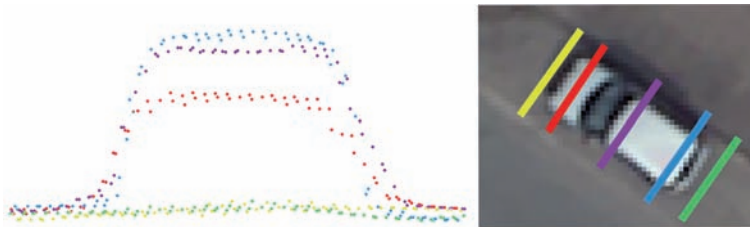


Fig. 7: Five profiles through a car in the SURE grid (OBLIQUE). Small transitions between street and car are clearly visible. The car length is about 3.5 m, its height above the street is about 1.3 m.

Tab. 1: Terrain coverage of the ALS and DIM points in study area Weser. ‘abs.’ is the absolute count of raster cells classified as terrain. ‘rel.’ is that count in relation to the count of raster cells ($4 \cdot 10^6$) in the whole study area. The raster width is 75 cm. The ALS points were classified using the interval $[-15, 15]$ cm, the DIM points using $[-150, 20]$ cm.

Method	abs.	rel. [%]
ALS	3283901	82.1
SURE (OBLIQUE)	2583479	64.6
SURE (DEFAULT)	2487792	62.2
SURE (AERIAL8080)	2456907	61.4
Match-T (UAS)	2263574	56.6
Match-T (85705570q)	2276512	56.9

terrain because of e.g. parking cars or because a new house was built after the ALS flight.

Note that because the distribution of the height differences is skewed this classification interval will tend to classify a bit too many DIM points as terrain. However, as we will see later in section 3.3, ALS still has a much larger degree of terrain coverage and therefore the general result is not affected by this tendency.

3.3 Terrain Coverage

For determining the degree of terrain coverage a raster with a certain cell size cs is defined in the study area. A raster cell is classified as terrain if it contains at least one terrain point. The degree of terrain coverage is then computed (i) absolutely using the number of cells that are classified as terrain and (ii) relatively using the ratio of that absolute number to the area size of the entire study area.

The cell size cs was chosen based on the density of the last echo points, which is 6 points/m². This corresponds to a point distance of 42 cm and thus would suggest a cell

size of 50 cm. Because of the variations in the sampling during laser scanning, some of these cells would not contain a single point and thus the terrain coverage for ALS would be unrepresentatively small. However, within such empty cells the heights could be interpolated easily from the points in the neighbouring cells, indicating that it is not necessary to demand an ALS point every 50 cm. Therefore, the cell size $cs = 75$ cm is chosen.

For this analysis all water areas are masked out. For this mask the union of the areas delineated as water in the ALS data (2011) and in the DIM data (2013) is computed. Thus, any raster cell that is within a water area in any of the delineation sets is excluded from the investigation, even if it was previously classified as terrain. In this way different water levels at both flight dates are compensated. Furthermore, in this mask the terrain changes between both dates mentioned in section 3.2.2 are integrated.

This method for determining the terrain coverage is applied to the previously classified ALS and DIM points. Tab. 1 contains the results. We see that for the whole study area Weser,

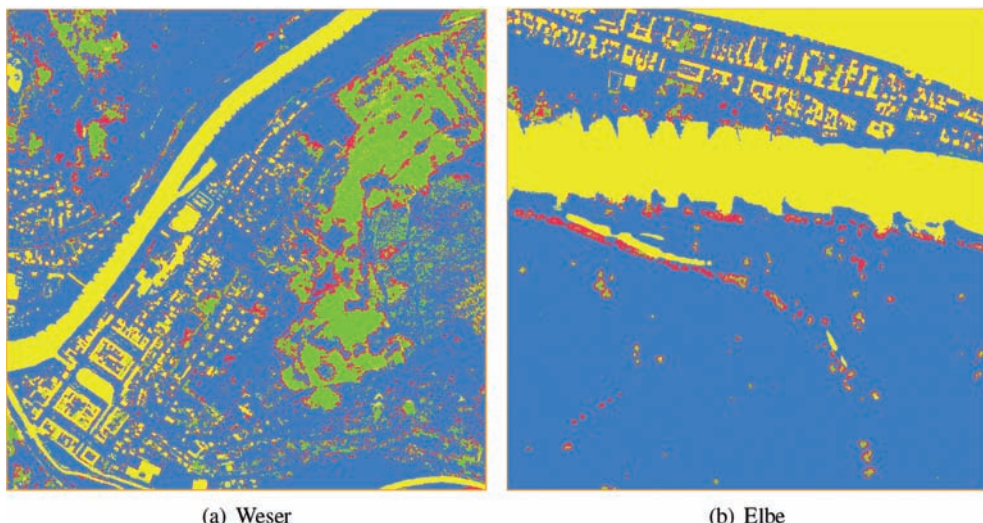


Fig. 8: Superimposition of the terrain coverages in study area Weser (left) and Elbe (right). Blue: Match-T + SURE + ALS, red: SURE + ALS, green: ALS. Yellow = Off-terrain or masked.

ALS gives a terrain coverage of 82 %, SURE of 65 % and Match-T of 57 %. ALS has the ability to penetrate vegetation and thus may serve as reference for the terrain coverage that can be achieved. In relation to that SURE delivers a quality of $65/82 = 78\%$, and Match-T a quality of $57/82 = 69\%$.

As mentioned in section 3.2.1 we also tested the intervals $[-10, 10]$ cm and $[-20, 20]$ cm for the ALS terrain classification. They result in relative terrain coverages of 81 % and 83 %, respectively. This shows that the choice of the classification interval has little influence on the ALS terrain coverage and we thus stick to the result obtained for the interval $[-15, 15]$ cm.

Fig. 8a shows a superimposition of the terrain coverage results for the entire study area Weser and Fig. 9b shows the result for a small section. The terrain coverage of Match-T (85705570 q) is shown in blue, below that is the result of SURE (OBLIQUE) in red and below that is the ALS result in green. Practically at each location where Match-T can deliver terrain heights so does SURE, and at each location where SURE can deliver so does ALS. Summarising, in red areas Match-T fails in comparison with SURE, and in green areas SURE fails in comparison with ALS.

It is clearly visible that in open areas SURE is able to deliver terrain heights closer to nearby

off-terrain objects than Match-T – but not as close as ALS. It is also apparent that in dense or high vegetation areas only ALS can deliver terrain heights.

In contrast to SURE, Match-T does not have any no-data areas. The explanation could be that Match-T is less strict in the acceptance of matched or interpolated heights than SURE.

3.4 Height Accuracy

The following two statistical values are computed for the height differences ΔZ : a location parameter, which measures a constant shift (e.g. caused by differences in the geodetic datum or by penetration depth) and a dispersion value, which measures the random deviations with respect to that location parameter. Both values are determined using the mentioned ΔZ histograms; see Figs. 5 and 6. Tab. 2 contains the following values for ALS and all DIM variants:

- The usual choices for the location parameter are mean or median. For real data generally the median is preferred, because it is more robust against blunders. In the present case the skewness in the histogram of ΔZ for DIM causes a slight displacement of the median. Therefore, also the mode is reported. The mode denotes the difference value ΔZ with the largest frequency, which, however,

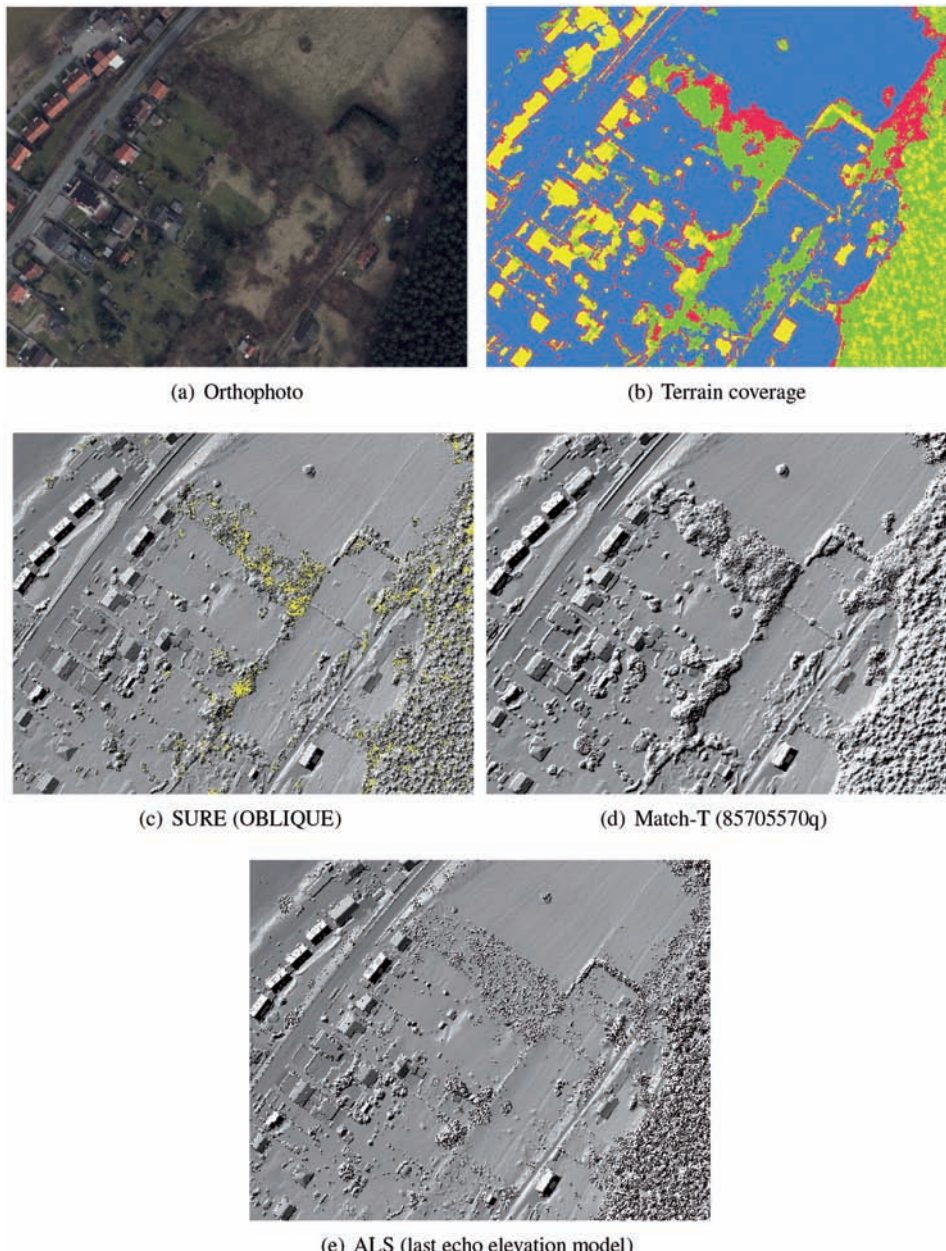


Fig. 9: Superimposition of the terrain coverages in the study area Weser (section). Blue: Match-T + SURE + ALS, red: SURE + ALS, green: ALS. Yellow = Off-terrain or masked. Additionally, the shadings of the respective grids are displayed. The east-west extension is about 330 m.

Tab. 2: Statistics of the height differences of all DIM variants in study area Weser with respect to the ALS-DTM in cm. The statistics of ALS tell how well the last echo points, which are classified as terrain, fit to the elevation model that was derived from them. All standard deviations refer to the mode, which is determined using a class width of 1.5 cm.

Method	Mean	Median	Mode	σ^-	σ^+	σ	RMS
ALS	0.4	0.2	-0.8	4.3	5.1	4.8	4.7
SURE (OBLIQUE)	3.5	2.5	0.8	5.0	7.7	6.9	7.1
SURE (DEFAULT)	4.8	3.2	0.8	5.1	8.0	7.2	7.5
SURE (AERIAL8080)	5.5	3.9	2.3	5.7	7.9	7.1	8.0
Match-T (UAS)	2.6	2.3	0.8	6.5	8.1	7.5	7.7
Match-T (85705570q)	3.1	2.2	0.8	5.2	8.0	7.0	7.3

for floating point samples can only be computed using classes. Here a class width of 1.5 cm was used. For all DIM variants the median is always below 4 cm and the mode is always below 2 cm. Thus, no considerable constant shift between ALS and the DIM results is present. The following three dispersion values refer to the mode.

- The standard deviation σ^- , which uses all ΔZ values within $[-20, 20]$ cm smaller than the mode. This value σ^- is representative for very smooth areas like sealed ground. For all DIM variants it is about 5 cm, which corresponds to half of the GSD.
- The standard deviation σ^+ , which uses all ΔZ values within $[-20, 20]$ cm larger than the mode. Because the histogram in Fig. 6 is skewed to the right this value σ^+ will be larger than σ^- in general. It is representative for terrain showing a bit of roughness, e.g. grassland or (bare) forest floor. For all DIM variants it is about 8 cm.
- The standard deviation σ , which is computed using all ΔZ values within $[-20, 20]$ cm. This value is an average of the previous two and for all DIM variants it is about 7 cm.
- Finally, also the root-mean-square (RMS) of all ΔZ values within $[-20, 20]$ cm is reported.

From Tab. 2 we see that SURE performs a bit better than Match-T and that the DIM statistics are only a little worse than the ALS results. From the RMS values we see, that the ALS points deviate by about 5 cm from the ALS-DTM, whereas the best DIM grid has a deviation of 7 cm.

4 Results for Study Area Elbe

For the second study area the very same methods as in section 3 were applied. Thus, only the main results are presented in the following.

4.1 Terrain Classification

A DTM is derived from the ALS data using all last echoes by means of a robust interpolation at a grid width of 0.5 m. Fig. 10 shows the histogram of the differences ΔZ of the last echoes to the DTM, limited to the interval $\text{abs}(\Delta Z) < 20$ cm. The ordinary standard deviation of these differences is 4.3 cm. The histogram is very similar to a Gaussian distribution. Based on that distribution the robust standard deviation σ_{MAD} is 3.9 cm and the median is 1.6 cm. The Gaussian distribution with these parameters is additionally drawn in Fig. 10, which fits to the histogram rather well, in contrast to the other study area Weser. This may be attributed to the very homogenous land cover, because 2/3 of study area Elbe are covered by grassland; see Fig. 2. In study area Weser the land coverage is much more diverse – especially the vegetation. All last echoes within $[-15, 15]$ cm are classified as terrain.

Fig. 11 shows the histogram of the DIM points of SURE (OBLIQUE) limited to $[-40, 40]$ cm. The median is 10.9 cm and σ_{MAD} is 5.4 cm. Compared to study area Weser (Fig. 5) two features are striking: (i) The Gaussian distribution using median and σ_{MAD} fits well to the histogram, which may be attributed again to the homogenous land cover. (ii) The median of 10.9 cm is significantly dif-

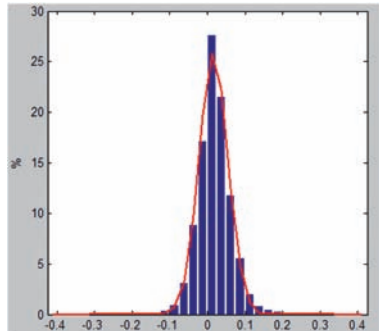


Fig. 10: Histogram of the height differences ΔZ (in m) of the last echoes to the ALS-DTM in study area Elbe; limited to $\text{abs}(\Delta Z) < 20$ cm. A Gaussian distribution with expectation 1.6 cm and standard deviation 3.9 cm is drawn in red.

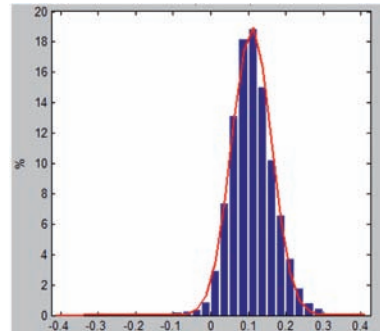
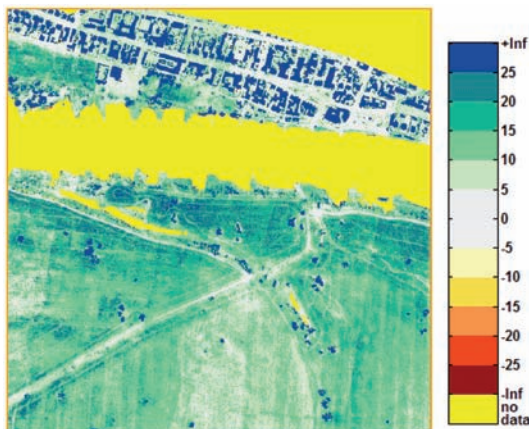


Fig. 11: Histogram of the height differences ΔZ (in m) of the SURE grid (OBLIQUE) to the ALS-DTM in study area Elbe; limited to $\text{abs}(\Delta Z) < 40$ cm. A Gaussian distribution with expectation 10.9 cm and standard deviation 5.4 cm is drawn in red.



(a) Height difference



(b) Analysis classes

Fig. 12: Study area Elbe. Left: Colour coding of the height difference SURE (OBLIQUE) minus ALS-DTM. The colour table is in cm. Big differences only occur in grass land. At sealed surfaces (especially streets) small differences prevail. Right: Classes used for grass height analysis (red = sealed, bright green = vegetation 1, dark green = vegetation 2, grey = remaining data, yellow = no data).

ferent from zero (significance level 0.05). This is not caused by an error in the geodetic datum. A closer examination reveals that this constant difference of 10.9 cm only appears at grassland, but not at sealed surfaces; see Fig. 12a. Because ALS and images were acquired simultaneously, the only explanation can be the different penetration behaviours of ALS and images. Whereas the last ALS echoes may orig-

inate from deeper grass layers or even the terrain, the images only see the top of the grass.

Consequently, this leaves two options: Either we do not accept this height error and get no photogrammetric heights in about 2/3 of the study area, or we accept it and get terrain points which are at a wrong height. This second option is chosen and thus the DIM points are classified using the interval $[-10, 30]$ cm.

Tab. 3: Terrain coverage of the ALS and DIM points in study area Elbe. ‘abs.’ is the absolute count of raster cells classified as terrain. ‘rel.’ is this count in relation to the count of raster cells ($1.778 \cdot 10^6$) in the whole study area. The raster width is 75 cm.

Method	abs.	rel. [%]
ALS	1318092	74.1
SURE (OBLIQUE)	1298434	73.0
SURE (DEFAULT)	1290578	72.5
SURE (AERIAL8080)	1283998	72.2
Match-T (UAS)	1244494	69.9
Match-T (8060)	1241591	69.8

Tab. 4: Statistics of the height differences of all DIM variants in study area Elbe with respect to the ALS-DTM in cm. The statistics of ALS just tell how well the last echo points, which are classified as terrain, fit to the elevation model that was derived from them. The standard deviation refers to the mean. The modi were determined using a class width of 1.5 cm.

Method	Mean	Median	Mode	σ	RMS
ALS	1.9	1.6	-0.8	4.3	4.7
SURE (OBLIQUE)	8.8	10.9	9.8	6.3	11.9
SURE (DEFAULT)	8.7	11.3	11.4	6.4	11.9
SURE (AERIAL8080)	9.6	12.1	11.4	6.5	12.6
Match-T (UAS)	10.8	10.4	9.8	5.8	12.1
Match-T (8060)	11.9	12.1	12.9	5.4	13.4

4.2 Terrain Coverage

The terrain coverage is determined again as in section 3.3 using a raster with cell size 75 cm. We also consider a mask to exclude water and no-data areas from our analysis. Fig. 8b and Tab. 3 show the results. We see that for the whole study area ALS gives a terrain coverage of about 74 %, SURE 73 % and Match-T 70 %. Using the ALS result as reference, SURE delivers a quality of $73/74 = 98.5\%$, and Match-T a quality of $70/74 = 97.2\%$. In contrast to study area Weser, DIM performs quite close to ALS, which is due to the high percentage of open grassland in the study area.

The problem areas for DIM are the same as in study area Weser (see Figs. 8a and 9). In open areas SURE is able to deliver terrain heights closer to nearby off-terrain objects than Match-T (red areas in Fig. 8b). In dense or high vegetation areas, of which there are only a few in study area Elbe, only ALS can deliver terrain heights (green areas in Fig. 8b).

4.3 Effect of Land Cover on Height Accuracy

As in section 3.4 dispersion and location parameter are derived from the ΔZ values with respect to the ALS-DTM using the intervals $[-20, 20]$ cm for ALS and $[-10, 30]$ cm for DIM; see Tab. 4. Since the histograms show no skewness at all only the ordinary standard deviation (with respect to the mean) and the RMS are given as dispersion values.

In section 4.1 the large offset of approximately 10 cm between DIM and ALS-DTM, which dominates also Tab. 4, was attributed to the different penetration behaviours of ALS and images. This offset is now analysed in two small areas of homogenous vegetation, which are shown in figure 12b in bright and dark green. They were selected using the orthophoto (Fig. 2) and the colour coded height difference (Fig. 12a). In order to judge this offset correctly any possible residual vertical datum error needs to be considered. Therefore, also the height differences in sealed areas are analysed, be-

Tab. 5: Statistics of the height differences of all DIM variants and the last echo points in study area Elbe with respect to the ALS-DTM in cm limited to sealed surfaces and two vegetation areas. The modi were determined using a class width of 1.5 cm.

Area	Method	Mean	Median	Mode	σ
sealed	ALS	2.8	2.6	3.0	5.5
	SURE (OBLIQUE)	4.8	4.7	3.8	3.0
	SURE (DEFAULT)	4.8	4.7	5.3	3.3
	SURE (AERIAL8080)	6.6	6.5	6.8	4.0
	Match-T (UAS)	5.6	5.5	5.3	4.5
	Match-T (8060)	5.6	5.4	5.3	3.6
vegetation 1	ALS	1.1	1.1	1.0	3.9
	SURE (OBLIQUE)	19.6	19.7	20.5	4.3
	SURE (DEFAULT)	20.8	20.9	20.5	4.6
	SURE (AERIAL8080)	18.2	18.4	18.9	4.7
	Match-T (UAS)	21.0	21.0	22.0	4.4
	Match-T (8060)	18.3	18.4	18.9	3.8
vegetation 2	ALS	2.1	2.1	1.0	4.3
	SURE (OBLIQUE)	16.4	16.8	17.4	5.5
	SURE (DEFAULT)	16.5	16.6	17.4	5.5
	SURE (AERIAL8080)	18.4	19.0	20.5	5.6
	Match-T (UAS)	17.2	17.9	20.5	5.7
	Match-T (8060)	17.5	18.2	20.5	5.2

cause there the penetration behaviours of ALS and images should be the same. The mask for the sealed areas (mostly asphalt) was digitized manually using the orthophoto and is shown in Fig. 12b in red.

Tab. 5 lists the ordinary standard deviation, the mean, the median and the mode (determined using class width 1.5 cm) for the ΔZ values of the ALS points and the DIM models with respect to the ALS-DTM within the sealed areas and the two vegetation areas. Because the location parameters, e.g. median, range between 3 cm and 20 cm, the median was computed first for the interval $[-10, 30]$ cm and afterwards the interval [median−20, median+20] cm was used for computing the listed statistical values.

Despite the smooth nature of the sealed surfaces their ALS statistics are a little worse than the ALS statistics in the vegetation areas. This is attributed to the asphalt coverage in the sealed areas. According to the ASTER spectral library (BALDRIDGE et al. 2009) the reflectance of near-infrared light for asphalt is around 10 %, whereas for green grass it is around 50 %. Con-

sequently, the signal to noise ratio and thus the distance measurement accuracy for asphalt (5.5 cm) will be worse than for grass (3.9 cm and 4.3 cm, respectively).

Interestingly, for sealed surfaces the accuracy of the DIM variants (with respect to the ALS-DTM) is better than for ALS itself. Here it is important to point out that the ALS accuracy refers to the original last echo points, whereas the DIM accuracy refers to an interpolated grid. Additionally, the DIM variants employ some sort of smoothness constraint. This constraint can be exploited to the full at the sealed areas, because they are planar and horizontal to a large degree (and thus parallel to the image bases). Consequently, the smoothness constraint allows to bridge the asphalt parts with low texture by propagating the heights from objects with high texture, e.g. road markings.

Over the sealed surfaces the DIM variants show a small constant offset of about 5 cm, which may be attributed to a small remaining error in the datum of the images with respect to ALS. Over the vegetation areas both ALS and

DIM show similar standard deviations, but the location parameters are very different because of the different penetration behaviours.

The grass height in both vegetation areas can be estimated by subtracting the location parameter (mean, median or mode) in the sealed surfaces from the one obtained in each vegetation area. All three location parameters are very similar, as the underlying distributions are close to a Gaussian. Therefore, based on the results for SURE (OBLIQUE) the grass height can be estimated to be about 15.5 cm in vegetation area 1 and about 12.5 cm in vegetation area 2.

From the standard deviations listed in Tab. 5 we see that SURE and Match-T perform practically identical in both vegetation areas, and both DIM results are a little worse than ALS. In the sealed area SURE is a bit better than Match-T and reaches half of the GSD as standard deviation. There ALS is actually worse than DIM due to the low reflectance of asphalt. In the vegetation areas DIM delivers points on the top of the grass, which is about 10 cm above the terrain.

5 Conclusions

The topic of this study was the comparison of airborne laser scanning (ALS) and dense image matching (DIM) regarding their potential for deriving terrain heights. Two study areas were considered and their results are quite consistent. Only ALS can reliably detect the terrain beneath vegetation. State of the art DIM is currently only able to achieve this in areas with no or only very loose vegetation. In such areas SURE delivers somewhat better results than Match-T. This dependence on the vegetation density is primarily supported by the results of study area Weser. There the vegetation structure is very diverse with respect to, both, stem density and tree types. Consequently, DIM only achieved 78 % of the terrain that ALS detected. But study area Elbe also shows an interesting result: Even in the case of open grassland (where DIM reached 98.5 % of the terrain that ALS detected) the terrain heights obtained by DIM cannot be fully trusted. The ALS terrain heights were systematically lower by about 10 cm. It is concluded that DIM provides systematically wrong (too high) terrain elevations

in such areas because matching occurs on top of the grass.

The very good height accuracy (as standard deviation) which can be achieved by DIM by exploiting the large image overlaps is encouraging. In both study areas the DIM height accuracy is only slightly worse than the ALS accuracy (6.5 cm vs. 4.5 cm). Specifically in smooth areas DIM can deliver heights with an accuracy of about half of the GSD.

Future developments in DIM may improve the matching quality of loosely vegetated terrain. However, because of the inherent occlusions caused even by leafless twigs, the terrain below loose vegetation will always be determined only by a small set of images with small base lines. Consequently, the reliability will be small and the height accuracy will be worse than presented here, where in the open areas the high image overlaps could be fully exploited.



Fig. 13: Dry fallen areas with groynes und groyne fields of river Rhine near Kaub.

On the other hand, in open areas with no or only very low grass coverage DIM can yield terrain data with high accuracy. Therefore, new possibilities arise for the BfG and the WSV, respectively, in the context of photogrammetric flights to be performed during periods of low discharge or for standardized high resolution mapping flights in dependence of given water levels and vegetation conditions. Ground data of groynes, groyne fields and other dry fallen areas of free flowing rivers, shown in Fig. 13, can be collected extensively on demand and efficiently with DIM. Furthermore, littoral zones can be captured at low water levels. These areas are difficult to collect by hydrographic measure-

ment systems, but they are predominantly open, supporting the use of DIM.

References

- AdV, 2013: Leitfaden Qualitätsstandard Airborne Laserscanning (QS-ALS), Version 1.1. – AK-Beschluss 26/12 der 26. Tagung des Arbeitskreises Geotopographie der Arbeitsgemeinschaft der Vermessungsverwaltungen der Länder der Bundesrepublik Deutschland.
- BALDRIDGE, A.M., HOOK, S., GROVE, C. & RIVERA, G., 2009: The ASTER Spectral Library Version 2.0. – *Remote Sensing of Environment* **113**: 711–715.
- BALTSAVIAS, E., 1999: A comparison between photogrammetry and laser scanning. – *ISPRS Journal of Photogrammetry and Remote Sensing* **54** (2–3): 83–94.
- BAUERHANSL, C., ROTTENSTEINER, F. & BRIESE, C., 2004: Determination of terrain models by digital image matching methods. – *International Archives of the Photogrammetry, Remote Sensing and Spatial Information Sciences* **35** (Part B4): 414–419, Istanbul, Turkey.
- HAALA, N. & ROTHERMEL, M., 2012: Dense multi-stereo matching for high quality digital elevation models. – PFG – Photogrammetrie, Fernerkundung, Geoinformation (4): 331–343.
- HAALA, N., HASTEDT, H., WOLF, K., RESSL, C. & BALTRUSCH, S., 2010: Digital photogrammetric camera evaluation – generation of digital elevation models. – PFG – Photogrammetrie, Fernerkundung, Geoinformation (2): 99–115.
- HIRSCHMÜLLER, H., 2008: Stereo processing by semi-global matching and mutual information. – *IEEE Transactions on Pattern Analysis and Machine Intelligence* **30** (2): 328–341.
- KRAUS, K. & PFEIFER, N., 1998: Determination of terrain models in wooded areas with airborne laser scanner data. – *ISPRS Journal of Photogrammetry and Remote Sensing* **53**: 193–203.
- LEBERL, F., GRUBER, M., PONTICELLI, M. & WIECHERT, A., 2012: The UltraCam story. – *International Archives of the Photogrammetry, Remote Sensing and Spatial Information Sciences* **39** (Part 1): 39–44, Melbourne, Australia.
- PETZOLD, B., REISS, P. & STÖSSEL, W., 1999: Laser scanning – surveying and mapping agencies are using a new technique for the derivation of digital terrain models. – *ISPRS Journal of Photogrammetry and Remote Sensing* **54** (2–3): 95–104.
- ROTHERMEL, M., WENZEL, K., FRITSCH, D. & HAALA, N., 2012: Sure: Photogrammetric surface reconstruction from imagery. – Low Cost 3D Workshop.
- SHAN, J. & TOTH, C.K. (ed.), 2008: *Topographic Laser Ranging and Scanning: Principles and Processing*. – CRC Press, Boca Raton, FL, USA.
- TRIMBLE, 2014: Match-T 5.5 Reference Manual.
- VÄSTARANTA, M., WULDER, M.A., WHITE, J.C., PEKKARINEN, A., TUOMINEN, S., GINZLER, C., KANKARE, V., HOLOPAINEN, M., HYYPÄ, J. & HYYPÄ, H., 2013: Airborne laser scanning and digital stereo imagery measures of forest structure: Comparative results and implications to forest mapping and inventory update. – *Canadian Journal of Remote Sensing* **39** (5): 382–395.
- VOSSELMAN, G., SESTER, M. & MAYER, H., 2004: Basic computer vision techniques. – J.C. McGLONE (ed.) – *Manual of Photogrammetry*. American Society for Photogrammetry and Remote Sensing, chapter **6**: 455–504.
- WEHR, A. & LOHR, U., 1999: Airborne laser scanning – an introduction and overview. – *ISPRS Journal of Photogrammetry and Remote Sensing* **54** (2–3): 68–82.
- XIAO, J., GERKE, M. & VOSSELMAN, G., 2012: Building extraction from oblique airborne imagery based on robust facade detection. – *ISPRS Journal of Photogrammetry and Remote Sensing* **68** (1): 56–68.
- ZABIH, R. & WOODFILL, J., 1994: Non-parametric local transforms for computing visual correspondence. – *Computer Vision ECCV '94, Lecture Notes in Computer Science*, Vol. **801**, Springer Berlin Heidelberg, 151–158.

Addresses of the Authors:

- Dr. CAMILLO RESSL, Technische Universität Wien, Department of Geodesy and Geoinformation, Gußhausstraße 27–29, A-1040 Vienna, Austria, e-mail: camillo.ressl@geo.tuwien.ac.at
- Dipl.-Ing. HERBERT BROCKMANN, Federal Institute of Hydrology, Department Geodesy, Am Mainzer Tor 1, D-56068 Koblenz, e-mail: brockmann@bafg.de
- Dr. GOTTFRIED MANDLBURGER, Technische Universität Wien, Department of Geodesy and Geoinformation, Gußhausstraße 27–29, A-1040 Vienna, Austria, e-mail: gottfried.mandlburger@geo.tuwien.ac.at
- Prof. Dr. NORBERT PFEIFER, Technische Universität Wien, Department of Geodesy and Geoinformation, Gußhausstraße 27–29, A-1040 Vienna, Austria, e-mail: norbert.pfeifer@geo.tuwien.ac.at

Manuskript eingereicht: September 2015

Angenommen: Januar 2016



Incidence Angle Dependency of Leaf Vegetation Indices from Hyperspectral Lidar Measurements

SANNA KAASALAINEN, OLLI NEVALAINEN, TEEMU HAKALA, Masala, Finland & KATI ANTTILA, Helsinki, Finland

Keywords: Hyperspectral, lidar, vegetation indices

Summary: We have studied the effect of incidence angle on the spectral content of leaf measurements from hyperspectral light detection and ranging (lidar) data. New results obtained for different ornamental plant leaves indicate that their backscatter properties do not follow the Lambert scattering law, especially in the visible wavelength range: specular reflections were observed near the normal incidence. Also the vegetation spectral indices, such as normalized difference vegetation index (NDVI), or even the simple ratios may change with the laser incidence angle to the target. The reason for this is the difference in their backscatter vs. intensity behaviour between visible and near-infrared (NIR) wavelengths. In comparison with earlier results it turns out that this phenomenon seems to depend on the internal structure and surface properties of leaves. Further information on the extent and role of this effect for different leaves is needed, but our results indicate that the nature of laser reflection in tree canopies may vary between species. The calibration of hyperspectral lidar vegetation reflectance measurements must be further studied by rigorous experiments and modelling.

Zusammenfassung: *Abhangigkeit von Vegetationsindices fur Blatter vom Inzidenzwinkel aus hyperspektralen Laserscanner-Messungen.* In diesem Beitrag wird der Einfluss des Einfallswinkels auf spektrale Indices, welche aus hyperspektralen Laserscanner-Messungen von Blattern abgeleitet werden, untersucht. Neue Ergebnisse fur Blatter von verschiedenen Zierpflanzen zeigen, dass deren Ruckstreuverhalten vor allem im sichtbaren Bereich des elektromagnetischen Spektrums nicht dem eines Lambertschen Strahlers entspricht: Bei genahert senkrechter Einfallrichtung wurde gerichtete Reflexion beobachtet. Auch spektrale Vegetationsindices wie z. B. der Normalized Difference Vegetation Index (NDVI) oder auch nur einfache Verhaltnisse konnen sich mit dem Einfallswinkel des Laserstrahls ndern. Der Grund dafr ist ein unterschiedliches Ruckstreuverhalten im sichtbaren Bereich bzw. im nahen Infrarot. Im Vergleich mit fruheren Ergebnissen scheint dieses Phanomen von der inneren Struktur und den Oberflacheneigenschaften der Blatter abzuhangen. Wrend tiefergehende Untersuchungen zum Ausma und zur Rolle dieses Effekts noch ausstehen, weisen unsere Ergebnisse darauf hin, dass die Art der Laserreflexion fr unterschiedliche Spezies variiieren konne. Die Kalibrierung von Reflexionsgraden aus multispektralen Laserscanner-Messungen erfordert weitere Studien in Hinblick auf eine strenge Modellierung und experimentelle Validierung.

1 Introduction

Photosynthetic activity in the tree canopy is a driver of growth and an indicator of tree health and productivity of plants in general. Trees with high foliar biomass and chlorophyll content have high carbon assimilation

capacity. Stress induces changes in photo-synthetically-active pigments (GITELSON & MERRILYAK 1994). Spectral indices are efficient in mapping the parameters related to vegetation health, water stress, and photosynthetic potential, because they are simple and easy to derive (WU et al. 2008, HOUORG & BOEGH 2008,

USTIN et al. 2004). Spectral remote sensing has been implemented at spatial resolution down to 40 cm (e.g. LAUSCH et al. 2013, KALACSKA et al. 2015). Improved resolution and more accurate 3D position for the spectra are still needed, because accurate leaf-level information on important vegetation parameters has thus far been available mainly from destructive measurements and representative sampling.

Spectral indices have traditionally been retrieved from passive spectral remote sensing (USTIN et al. 2004, LAUSCH et al. 2013, KALACSKA et al. 2015). Recently, multiwavelength terrestrial laser scanning has also been found to be a promising tool for combined structure and spectral measurement (GAULTON et al. 2013, NEVALAINEN et al. 2014, LI et al. 2014). The role of measurement geometry and the effects from laser interaction with complex structures (such as tree canopies) are not yet completely understood. The effect of the incidence angle, i.e., the angle between incoming laser beam and surface normal, on the laser scanning (intensity) data has been studied for leaves and different targets with monochromatic laser scanners, mainly for the purpose of calibrating or improving the laser scanning results (LICHTI 2005, PESCI & TEZA 2008, SOUDARISSANANE et al. 2011, BALDUZZI et al. 2011, KAASALAINEN et al. 2011). However, only a few studies have been carried out with multispectral or hyperspectral laser scanners. New results have emerged quite recently for dual wavelength light detection and ranging (lidar) measurements (GAULTON et al. 2013), but more information is needed on the effect of the incidence angle on spectral vegetation indices. This is partially because multispectral terrestrial laser scanners have been developed and applied only recently (DOUGLAS et al. 2012, HAKALA et al. 2012, DANSOON et al. 2014, LI et al. 2014). A multispectral canopy lidar has been introduced by WOODHOUSE et al. (2011) for simultaneous retrieval of vegetation profiles and spectral indices at the canopy scale.

It has been assumed in previous studies that spectral ratios should be insensitive to the incidence angle because the backscattered intensity for each index has been measured at similar geometry. Leaves are commonly assumed to be close to Lambertian scatterers. Therefore, the spectral ratios should be pri-

marily affected by the target spectral reflectance only (GAULTON et al. 2013). In their experiment for deciduous leaves with a 4-channel multispectral lidar, SHI et al. (2015) found the influence of the incidence angle to be similar in all wavelengths for a deciduous leaf, and subsequently, no effect on a spectral ratio was observed. Conversely, EITEL et al. (2014) found the specular reflection to play an important role.

Leaf optical properties have been modelled with, e.g., the PROSPECT model from passive or simulated hyperspectral data (MORSDORF et al. 2009, WANG et al. 2015). EITEL et al. (2010, 2011) studied the relationship between foliar nitrogen and chlorophyll concentrations and laser return intensity with a green laser (532 nm) and found that the variations in leaf angles (and hence the incidence angle) complicated the predictions. ZOU et al. (2014) reported a high correlation between canopy reflectance in the red edge (at 748 nm) and leaf mean tilt angles. Thus, there is a growing need for systematic experiments on the effects of leaf geometry and structure on laser return intensity and canopy reflectance in general. Especially, the role of multiple scattering and the influence of structural change on the retrieval of vegetation indices should be studied in more detail.

The main goal of this paper is to explore the effect of measurement geometry on vegetation indices retrieved with a hyperspectral lidar instrument. We study the effect of incidence angle on laser backscatter from leaves at different wavelengths and discuss the effect of the results on the future research on vegetation 3D spectral remote sensing.

2 Material and Methods

2.1 Laser Scanner Intensity

The radar equation defines the power (P_r) received by a laser scanner detector to be:

$$P_r = \frac{P_t D_r^2}{4\pi R^4 \beta_t^2} \sigma , \quad (1)$$

where P_t is the transmitted power, D_r is the receiver aperture, R is the range, and β_t is the transmitter beam width. σ is the backscatter cross section (HÖFLE & PFEIFER 2007), which depends on the measurement geometry as follows:

$$\sigma = \frac{4\pi}{\Omega} \rho A_s . \quad (2)$$

ρ is the reflectivity of the scatterer and Ω is the scattering solid angle. A_s is the illuminated area of the scattering element, which is a function of range R and beam width β_t :

$$A_s = \frac{\pi R^2 \beta_t^2}{4} . \quad (3)$$

Substituting this into (2), we get the backscatter cross section in the form:

$$\sigma = \pi \rho R^2 \beta_t^2 \cos \alpha , \quad (4)$$

where α is the laser incidence angle to the target (SHAKER et al. 2011). In our study, all parameters, including the range R , remained constant, except for σ , which depends on the incidence angle α (KAASALAINEN et al. 2011). MORSDORF et al. (2009) modelled the laser return signal from leaves with the PROSPECT model, where the leaves were assumed to be Lambertian scatterers. So the directional component ($4\pi/\Omega$) in (2), could be neglected. This is the starting point of our study, as we can now investigate the leaf spectra at different incidence angles (α) with a hyperspectral lidar instrument.

Tab. 1: The HSL characteristics (FWHM = Full Width at Half Maximum).

Wavelength channels	555, 624, 691, 726, 760, 795, 899, 1000 nm
Optical bandpass	20 nm (FWHM)
Pulse rate	5.3 kHz
Pulse length	1 ns
Average output power	41 mW
Beam diameter	4 mm at exit
Beam divergence	~0.02° at 543 nm
Range resolution	15 cm
Scan speed	Max 60°/s (vertical)

2.2 The Instrument and Measurements

The Hyperspectral Lidar (HSL) is a prototype multi-wavelength laser scanner with a supercontinuum laser light source (420 nm – 2400 nm). It produces a 3D point cloud with a spectrum associated to each point. A laser pulse is transmitted to a target and the range is measured from the time for the reflected pulse to return. The HSL uses a spectrograph and a 16-element avalanche photodiode (APD) array as a detector, connected to a high-speed (1 ns sampling rate) 8-channel digitizer. The intensity of each transmitted laser pulse is measured and used to normalize the intensity of the backscattered laser pulse. The sensor has also been calibrated with respect to the measured distances separately for each wavelength. The digitizer enables data storage at 8 wavelength bands. These bands can be selected by adjusting the position of the dispersion from the spectrograph with respect to the APD array. In this study, the wavelength channels were 555, 624, 691, 726, 760, 795, 899 and 1000 nm (see Tab. 1). The rose sample was measured separately after some modifications had been made to the instrument. Therefore, the channels were slightly different (section 2.3). A Spectralon® reference target with 99% nominal reflectance was measured at the same distance as the leaf targets. The instrument and data processing are presented in more detail in HAKALA et al. (2012).

The leaf samples were taken from three common ornamental plants: Chinese hibiscus

(*Hibiscus rosa-sinensis*), a widely used flower in pharmacology (e.g. SHARMA & SULTANA 2004), Zamioculcas (Common name “Zanzibar Gem”) (*Zamioculcas zamiifolia*), a tropical perennial, and a rose (*Rosa spp.*) sample commonly available in florist shops. We also scanned a sand sample taken from a beach in Kivenlahti, Finland, which was sieved into 500 mm grain size. This sample has also been measured in earlier experiments with a monochromatic laser scanner, so it provided an important reference (KROOKS et al. 2013).

All measurements were carried out indoors under laboratory conditions. The leaf samples were placed on a motorized rotating platform at about 4-metre distance from the scanner. The incidence angle was changed in 5° increments, and a scan over the leaf was performed at each incidence angle.

2.3 Data Processing and Analysis

The measured HSL point clouds were processed using MATLAB 2013a software (The MathWorks®, Inc.). Laser echoes from outside the leaf were manually removed from the point clouds. The mean backscattered reflectance of all the echoes from the leaf was used as the backscattered reflectance at each incidence angle.

The spectral indices compared in this study are commonly used in retrieving vegetation characteristics, such as leaf chlorophyll or nitrogen content (see also NEVALAINEN et al. 2014). The chlorophyll concentration is related to plant photo-synthetic potential and senescing (GITELSON & MERZLYAK 1994), and therefore the reliability of its measurement is crucial.

The normalized difference vegetation index (NDVI) is based on the contrast between high chlorophyll absorption at red and high reflectance (R) at near-infrared (TUCKER 1979, WU et al. 2008). It has also been used for mapping leaf-area index (HOBORG & BOEGH 2008) and chlorophyll concentration (WU et al. 2008). The wave-length channels used in this study were 691 nm in the red and 795 nm in NIR:

$$NDVI = \frac{R_{795} - R_{691}}{R_{795} + R_{691}} \quad (5)$$

We also compared the Red Edge Normalized Difference Vegetation Index (GITELSON & MERZLYAK 1994), where the wavelength channels were 760 nm and 726 nm, respectively (764 nm and 713 nm for the rose).

Promising results in leaf-level chlorophyll (Cab) estimation have been obtained with the so-called red edge and spectral and derivative indices such as R750/R710 (ZARCO-TEJADA et al. 2004). This index is also called the single ratio or simple ratio (SR). A variety of wavelength combinations can be used, but we selected R760/R726 to calculate the ratio (R764/R713 for the rose sample).

The modified simple ratio MSR has been used to estimate chlorophyll and leaf area index (LAI) at canopy scale (WU et al. 2008):

$$MSR = \frac{\frac{R_{750}}{R_{705}} - 1}{\sqrt{\frac{R_{750}}{R_{705}} + 1}} \quad (6)$$

In this study, we used reflectances at 760 nm and 691 nm, which were closest to those in (6), for computing the MSR (764 nm and 713 nm for the rose sample, respectively) in (6).

We also included the modified chlorophyll absorption ratio index using reflectance at 705 nm and 750 nm (referred here as MCARI750) and defined as follows (WU et al. 2008):

In this paper, the reflectances at 760 nm, 691 nm (764 nm and 713 nm for the rose leaf sample), and 555 nm (561 nm for the rose) were used for the MCARI.

$$MCARI[705,750] = \left[(R_{750} - R_{705}) - 0.2 \times (R_{750} - R_{555}) \right] \left(\frac{R_{750}}{R_{705}} \right) \quad (7)$$

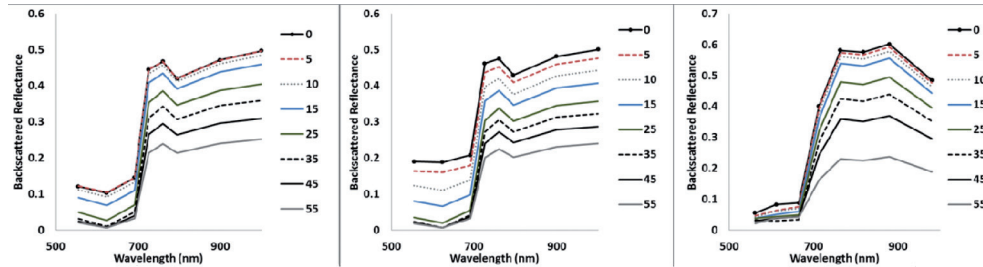


Fig. 1: Spectra vs. incidence angle. Left: Zanzibar Gem, middle: Chinese Hibiscus, right: Rose leaf.

3 Results

3.1 Incidence Angle vs. Wavelength

The spectra at different incidence angles for all samples are presented in Fig. 1. The spectral shape remains the same otherwise, but the decline in intensity from 0° towards larger incidence angles is sharper in the visible than in the NIR spectral range. This can also be seen in the incidence angle vs. intensity curves pre-

sented in Fig. 2. The intensity decline between 0° and 40° is presented in Tabs. 2 – 3, where it can also be observed that it is prominent in the visible, but not so sharp in the NIR range. This is clearly seen in Fig. 3, where the intensities of the Zanzibar Gem sample have been normalized to 1 at 0° .

In spite of the obviously non-lambertian intensity vs. incidence behaviour in the visible range, we examined this feature a little further for the Zanzibar Gem sample, by fitting a

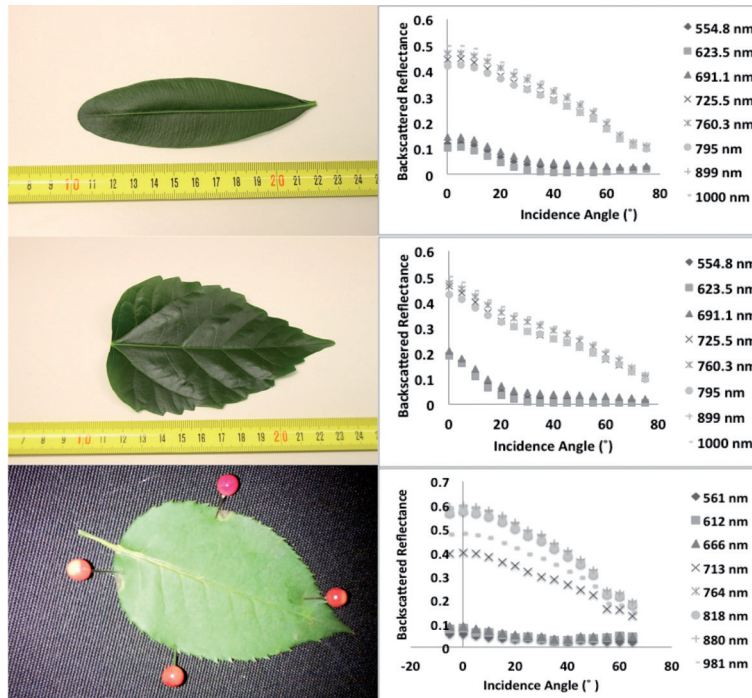


Fig. 2: The samples (left) and their incidence angle vs. backscattered reflectance (right) at all eight wavelength channels: top: Zamioculcas (Zanzibar Gem), middle: Chinese hibiscus, bottom: Rose. The pinheads are 5 mm in diameter.

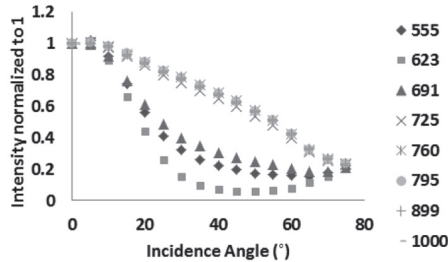


Fig. 3: Intensity normalized to 1 at 0° for the Zanzibar Gem sample.

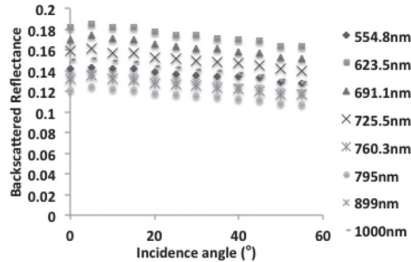


Fig. 5: Backscattered laser reflectance vs. incidence angle for beach sand, sieved into 500 µm grain size.

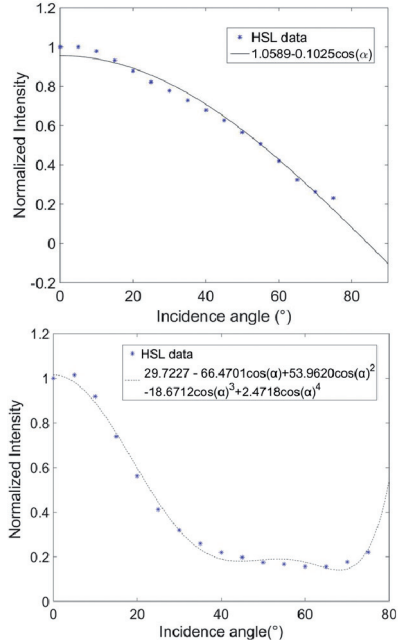


Fig. 4: Intensity normalized to 1 at 0° at 795 nm (top) and 555 nm (bottom) for the Zanzibar Gem sample (Fig. 3), with the n'th order cosine function ((2), with $n = 1$ and $n = 4$, respectively) plotted to the data.

cosine function (4), where the term $\pi\rho R^4 \beta_t^2$ was assumed constant, as all measurements were carried out at the same distance. The results for visible (555 nm) and near-infrared (795 nm) case are shown in Fig. 4. The R^2 coefficient of determination for this fit was 0.98 (with 0.031 RMSE), which indicates a good fit in the NIR case. For 555 nm, the R^2 was 0.58, and therefore we fitted the 4th power of the cosine function (Fig. 4) to obtain a better fit with $R^2 = 0.99$ and RMSE 0.023. It appears that at visible wavelengths the scattering does not follow the 1st order cosine function.

The Kivenlahti sand sample (Fig. 5), measured in the same experiment, showed similar incidence angle vs. intensity behaviour as in our earlier study with a monochromatic laser scanner (KROOKS et al. 2013). The decline between 0° and 40° was about 5% – 6% in visible and 6% – 8% in NIR. This means that for the sand sample, the effect of the incidence angle to the spectral shape is smaller than for the leaves.

Tab. 2: The decrease in intensity between 0° and 40° incidence angles for Zanzibar Gem at all wavelengths.

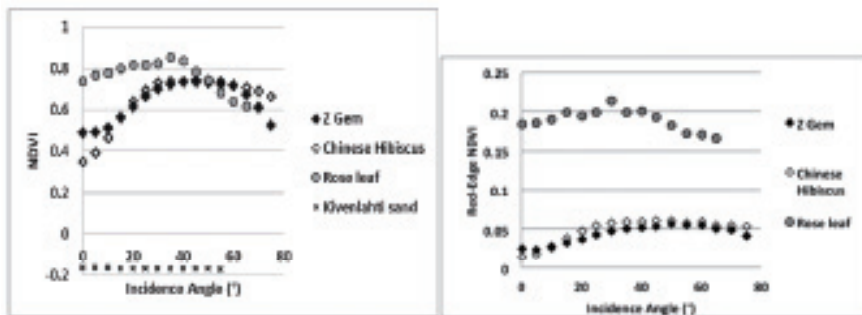
Wavelength (nm)	$I(0^\circ)$	$I(40^\circ)$	Drop in %
555	0.12	0.03	78
624	0.10	0.007	93
691	0.14	0.04	70
726	0.44	0.29	35
760	0.47	0.32	32
795	0.42	0.29	32
899	0.47	0.32	32
1000	0.50	0.33	33

Tab. 3: As in Tab. 2, for Chinese Hibiscus.

Wavelength (nm)	$I(0^\circ)$	$I(40^\circ)$	Drop in %
555	0.19	0.02	89
624	0.19	0.006	97
691	0.21	0.04	81
726	0.46	0.26	47
760	0.47	0.32	39
795	0.43	0.26	40
899	0.48	0.29	39
1000	0.50	0.30	40

Tab. 4: As in Tab. 2, for Rose.

Wavelength (nm)	$I(0^\circ)$	$I(40^\circ)$	Drop in %
561	0.05	0.03	53
612	0.08	0.03	65
666	0.08	0.03	61
713	0.40	0.26	34
764	0.58	0.39	32
818	0.58	0.38	33
880	0.60	0.41	32
981	0.48	0.32	33

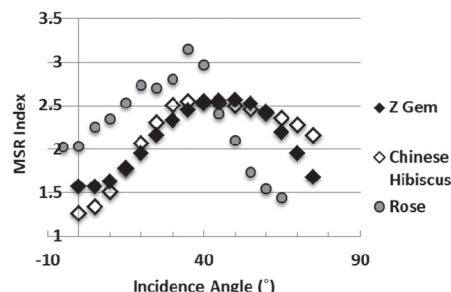
**Fig. 6:** Left: The NDVI index vs. incidence angle for leaf and beach sand samples. Right: the red-edge NDVI for leaf samples.

3.2 The Spectral Indices

Comparison of the NDVI, simple ratio, MSR, and the MCARI[705,750] indices for all leaves are presented in Figs. 6 – 9. The NDVI index has also been plotted in Fig. 6 for the sand sample, to show the difference in results with those for the leaves.

A clear incidence angle effect is observed for all four indices, and for all leaf samples, which is not monotonic. The sharpest changes are observed at incidence angles less than 20°. The changes at incidence angles greater than 60° may be caused by inaccuracies caused by the high tilt angle of the leaves, resulting in

the laser echo mixing with the surroundings. It was also found in BALDUZZI et al. (2011) that results for pear tree leaves were inaccurate at

**Fig. 7:** The MSR index vs. incidence angle.

incidence angles greater than 60°, which was also accounted for mixed intensities at high angles of incidence.

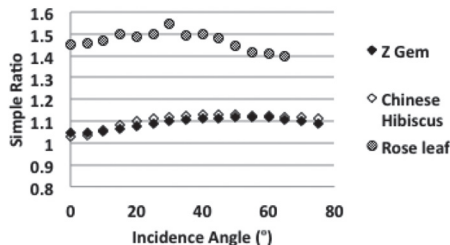


Fig. 8: The simple ratio: R760/R726 for waxed leaves, R764/713 for the rose sample.

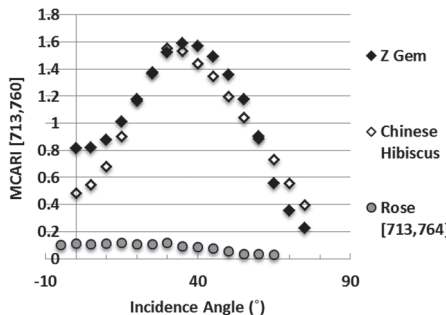


Fig. 9: MCARI[691,760] index for Zanzibar Gem and Chinese Hibiscus, and MCARI[713,764] for the rose leaf sample.

4 Discussion

The results are similar to those obtained by LICHTI (2005), who compared the lidar intensity vs. incidence angle in the near-infrared for different targets and observed a sharp (about 55%) decrease between 0° and 20° in the intensity of a matt black plastic. This was suggested to be due to its partially specular reflectivity, since the decrease was much less steep for other targets (such as tile). In our results, the intensity curves in Fig. 2 suggest a specular reflection, which is likely to be caused by the waxed surface of the leaf samples, especially for the Chinese Hibiscus. The specular reflection is pronounced in the visible (especially red) wavelengths, where the leaf reflectance is low (Fig. 3). For the rose leaf, the specular reflection is not as prominent as for the two waxed leaf samples, but the decrease

between 0° and 20° was 39% at 561 nm, while it was about 3% for the sand sample (Fig. 5).

No signs of specular reflection were found for an oriental plane (*Platanus orientalis*) leaf sample by SHI et al. (2013). The results obtained by BALDUZZI et al. (2011) for conference pear (*Pyrus Communis*) tree leaves at 785 nm did not show any strong specular reflection either. This result is similar to ours at NIR wavelengths, but more leaf types with different surface properties and internal structure should be studied to understand the role of specular reflection in the visible part of the spectrum. Also, the influence of the laser footprint size should be investigated, as the beam divergence is known to increase with increasing wavelength. We carried out the distance calibration separately at each wavelength to reduce the effect of laser spot size.

Although these results are preliminary, they confirm the role of laser incidence to the target and laser reflection in the canopy that must be taken into account when measuring vegetation indices with laser scanning.

In a 3D measurement over a large and complex target, such as a tree, there are multiple echoes resulting from laser hits to more than one leaf/needle. The leaf curvature, angular distribution, and other shape irregularities are likely to average the effect of incidence angle, at least in the tree scale. This, however, must be better characterized in future experiments, particularly in the spectral red edge and NIR spectral regions.

5 Conclusion

We have studied vegetation spectral indices with hyperspectral laser scanning and found that they change with the laser incidence angle to the target.

These results call for an extensive study of multispectral laser vegetation indices to get a better understanding of their sensitivity to variations in the leaf angle distribution. In the future, hyperspectral laser scanning will enable the retrieval of quantitative 3D/4D distributions of plant eco-physiological variables from vegetation indices. A better understanding of scattering effects on vegetation indices would improve the reliability of the measure-

ment, so that the indices can be accurately mapped over an entire tree instead of sampling individual leaves.

Future research will include more leaf types and varying measurement geometries. More information on the role of measurement geometry in laser scanning of vegetation canopies can then be obtained by modelling the leaf-laser interaction with a leaf scattering model (such as the PROSPECT), effects of shoot and canopy structure on laser backscatter, and including a large set of leaf/needle types. The leaf scattering models also need to be upgraded to simulate specular reflectance.

Acknowledgements

This study was funded by the Academy of Finland research project “Mobile hyperspectral laser remote sensing”.

References

- BALDUZZI, M.A.F., VAN DER ZANDE, D., STUCKENS, J., VERSTRAETEN, W.W. & COPPIN, P., 2011: The Properties of Terrestrial Laser System Intensity for Measuring Leaf Geometries: A Case Study with Conference Pear Trees (*Pyrus Communis*). – *Sensors* **11** (12): 1657–1681.
- DANSON, F.M., GAULTON, R., ARMITAGE, R.P., DISNEY, M., GUNAWAN, O., LEWIS, P. & RAMIREZ, A. F., 2014: Developing a dual-wavelength full-waveform terrestrial laser scanner to characterize forest canopy structure. – *Agricultural and Forest Meteorology* **198–199**: 7–14.
- DOUGLAS, E.S., STRAHLER, A., MARTEL, J., COOK, T., MENDILLO, C., MARSHALL, R., CHAKRABARTI, S., SCHAAF, C., WOODCOCK, C., LI, Z., YANG, X., CULVENOR, D., JUPP, D., NEWNHAM, G. & LOVELL, J., 2012: DWEL: A Dual-Wavelength Echidna Lidar for ground-based forest scanning. – *IEEE IGARSS*: 4998–5001.
- EITEL, J.U.H., VIERLING, L.A. & LONG, D.S., 2010: Simultaneous measurements of plant structure and chlorophyll content in broadleaf samplings with a terrestrial laser scanner. – *Remote Sensing of Environment* **114** (10): 2229–2237.
- EITEL, J.U.H., VIERLING, L.A., LONG, D.S. & HUNT, E.R., 2011: Early season remote sensing of wheat nitrogen status using a green scanning laser. – *Agricultural and Forest Meteorology* **151** (10): 1338–1345.
- EITEL, J.U.H., MAGNEY, T.S., VIERLING, L.A. & DITTMAR, G., 2014: Assessment of crop foliar nitrogen using a novel dual-wavelength laser system and implications for conducting laser-based plant physiology. – *ISPRS Journal of Photogrammetry and Remote Sensing* **97**: 229–240.
- GAULTON, R., DANSON, F.M., RAMIREZ, F.A. & GUNAWAN, O., 2013: The potential of dual-wavelength laser scanning for estimating vegetation moisture content. – *Remote Sensing of Environment* **132**: 32–39.
- GITELSON, A. & MERZLYAK, M.N., 1994: Spectral Reflectance Changes Associated with Autumn Senescence of *Aesculus hippocastanum* L. and *Acer platanoides* L. Leaves. Spectral Features and Relation to Chlorophyll Estimation. – *Journal of Plant Physiology* **143** (3): 286–292.
- HAKALA, T., SUOMALAINEN, J., KAASALAINEN, S. & CHEN, Y., 2012: Full waveform hyperspectral LiDAR for terrestrial laser scanning. – *Optics Express* **20** (7): 7119–7127.
- HOUBORG, R. & BOEGH, E., 2008: Mapping leaf chlorophyll and leaf area index using inverse and forward canopy reflectance modeling and SPOT reflectance data. – *Remote Sensing of Environment* **112** (1): 186–202.
- HÖFLE, B. & PFEIFER, N., 2007: Correction of laser scanning intensity data: Data and model-driven approaches. – *ISPRS Journal of Photogrammetry and Remote Sensing* **62** (6): 415–433.
- KAASALAINEN, S., JAAKKOLA, A., KAASALAINEN, M., KROOKS, A. & KUKKO, A., 2011: Analysis of Incidence Angle and Distance Effects on Terrestrial Laser Scanner Intensity: Search for Correction Methods. – *Remote Sensing* **3** (12): 2207–2221.
- KALACKA, M., LALONDE, M. & MOORE, T.R., 2015: Estimation of foliar chlorophyll and nitrogen content in an ombrotrophic bog from hyperspectral data: scaling from leaf to image. – *Remote Sensing of Environment* **169**: 270–279.
- KROOKS, A., KAASALAINEN, S., HAKALA, T. & NEVALAINEN, O., 2013: Correction of Intensity Incidence Angle Effect in Terrestrial Laser Scanning. – *ISPRS Annals of the Photogrammetry, Remote Sensing and Spatial Information Sciences II-5 (W2)*: 145–150.
- LAUSCH, A., HEURICH, M., GORDALLA, D., DOBNER, H.-J., GWILLYM-MARGIANTO, S. & SALBACH, C., 2013: Forecasting potential bark beetle outbreaks based on spruce forest vitality using hyperspectral remote-sensing techniques at different scales. – *Forest Ecology and Management* **308**: 76–89.
- LI, W., SUN, G., NIU, Z., GAO, S. & QIAO, H., 2014: Estimation of leaf biochemical content using a novel hyperspectral full-waveform LiDAR system. – *Remote Sensing Letters* **5** (8): 693–702.

- LICHTI, D.D., 2005: Spectral Filtering and Classification of Terrestrial Laser Scanner Point Clouds. – *The Photogrammetric Record* **20** (111): 218–240.
- MORSDORF, F., NICHOL, C., MALTHUS, T. & WOODHOUSE, I.H., 2009: Assessing forest structural and physiological information content of multispectral LiDAR waveforms by radiative transfer modelling. – *Remote Sensing of Environment* **113** (10): 2152–2163.
- NEVALAINEN, O., HAKALA, T., SUOMALAINEN, J., MÄKIPÄÄ, R., PELTONIEMI, M., KROOKS, A. & KAASALAINEN, S., 2014: Fast and nondestructive method for leaf level chlorophyll estimation using hyperspectral LiDAR. – *Agricultural and Forest Meteorology* **198–199**: 250–258.
- PESCI, A. & TEZA, G., 2008: Effects of surface irregularities on intensity data from laser scanning: an experimental approach. – *Annals of Geophysics* **51** (5–6): 839–848.
- SHAKER, A., YAN, W.Y. & EL-ASHMAWY, N., 2011: The effects of laser reflection angle on radiometric correction of the airborne lidar intensity data. – *The International Archives of the Photogrammetry, Remote Sensing and Spatial Information Sciences* **38** (5/W12): 213–217.
- SHARMA, S. & SULTANA, S., 2004: Effect of Hibiscus rosa sinensis Extract on Hyperproliferation and Oxidative Damage Caused by Benzoyl Peroxide and Ultraviolet Radiations in Mouse Skin. – *Basic & Clinical Pharmacology & Toxicology* **95** (5): 220–225.
- SHI, S., SONG, S., GONG, W., DU, L., ZHU, B. & HUANG, X., 2015: Improving Backscatter Intensity Calibration for Multispectral LiDAR. – *IEEE Geoscience and Remote Sensing Letters* **12** (7): 1421–1425.
- SOUADARISSANANE, S., LINDENBERGH, R., MENENTI, M. & TEUNISSEN, P., 2011: Scanning geometry: Influencing factor on the quality of terrestrial laser scanning points. – *ISPRS Journal of Photogrammetry and Remote Sensing* **66** (4): 389–399.
- TUCKER, C.J., 1979: Red and Photographic Infrared Linear Combinations for Monitoring Vegetation. – *Remote Sensing of Environment* **8** (2): 127–150.
- USTIN, S.L., ROBERTS, D.A., GAMON, J.A., ASNER, G.P. & GREEN, R.O., 2004: Using Imaging Spectroscopy to Study Ecosystem Processes and Properties. – *BioScience* **54** (6): 523–534.
- WANG, Z., SKIDMORE, A.K., WANG, T., DARVISHZADEH, R. & HEARNE, J., 2015: Applicability of the PROSPECT model for estimating protein and cellulose+lignin in fresh leaves. – *Remote Sensing of Environment* **168**: 205–218.
- WOODHOUSE, I.H., NICHOL, C., SINCLAIR, P., JACK, J., MORSDORF, F., MALTHUS, T.J. & PATENAUME, G., 2011: A Multispectral Canopy LiDAR Demonstrator Project. – *IEEE Geoscience and Remote Sensing Letters* **8** (5): 839–843.
- WU, C., NIU, Z., TANG, Q. & HUANG, W., 2008: Estimating chlorophyll content from hyperspectral vegetation indices: Modeling and validation. – *Agricultural and Forest Meteorology* **148** (8–9): 1230–1241.
- ZARCO-TEJADA, P., MILLER, J., MORALES, A., BERJÓN, A. & AGÜERA, J., 2004: Hyperspectral indices and model simulation for chlorophyll estimation in open-canopy tree crops. – *Remote Sensing of Environment* **90** (4): 463–476.
- ZOU, X., MÖTTUS, M., TAMMEORG, P., TORRES, C.L., TAKALA, T., PISEK, J., MÄKELÄ, P., STODDARD, F.L. & PELLIKKA, P., 2014: Photographic measurement of leaf angles in field crops. – *Agricultural and Forest Meteorology* **184**: 137–146.
- Address of the Authors:
 Dr. SANNA KAASALAINEN, OLLI NEVALAINEN & TEEMU HAKALA, Finnish Geospatial Research Institute–FGI, Masala, Finland. Tel +358-50-3696806, e-mail: {sanna.kaasalainen@}{olli.nevalainen}{teemu.hakala}@nls.fi
 KATI ANTILA, FINNISH Meteorological Institute (FMI), Helsinki, Finland. Tel.: +358-50- 4412298, e-mail: kati.antila@fmi
- Manuskript eingereicht: September 2015
 Angenommen: Januar 2016



A Comparison of UAV- and TLS-derived Plant Height for Crop Monitoring: Using Polygon Grids for the Analysis of Crop Surface Models (CSMs)

GEORG BARETH, JULIANE BENDIG, NORA TILLY, DIRK HOFFMEISTER, HELGE AASEN & ANDREAS BOLTEN, Cologne

Keywords: oktcopter, laserscanning, SfM, biomass, zonal statistics

Summary: Multi-temporal crop surface models (CSMs) are a reliable method for agricultural crop monitoring. They provide 3-dimensional representations of crop canopies, preferably available as a multi-temporal dataset. From the CSMs the spatial distribution of plant height can be derived. The data for the CSMs are captured by remote sensing methods including terrestrial laser scanning (TLS) and imagery from unmanned aerial vehicles (UAVs) combined with computer vision techniques. Previous studies underlined the suitability of both methods. However, it remained an open question if both methods provide actually comparable information. We assume that the differing viewing angles of both sensors influence the resulting CSM and that the UAV-based CSMs contain crop density information due to the nadir sensor position. Therefore, we expect a lower mean plant height and higher variation in the UAV-based CSM. The correlation between plant heights from both methods was analyzed and complemented by using polygon grids for spatial analysis. The polygon grids provide descriptive statistics for each raster cell by zonal statistics to investigate the data's potential as a density measure. Through this analysis it is possible to maximize the extraction of spatial information for larger grid cells though it is not comparable to standard resampling methods. We analyzed CSMs at early, middle, and late growth stages from a barley experiment field and found a high correlation ($R^2 = 0.91$) in plant height derived from both methods. The UAV-derived plant height was generally lower than the TLS-derived plant height at all growth stages. However, contrary to the expectations the coefficient of variation was higher in the TLS dataset.

Zusammenfassung: Vergleich von UAV- und TLS-abgeleiteter Pflanzenhöhe für das Monitoring von Ackerfrüchten: Die Nutzung von Polygongrids zur Analyse von Oberflächenmodellen von Getreidebeständen (CSMs). Oberflächenmodelle von Getrei-

debeständen (*crop surface models*, CSMs) sind eine zuverlässige Methode für das Agrarmonitoring. Sie ermöglichen die Erstellung dreidimensionaler Modelle geschlossener Getreidebestände, vorzugsweise aus multitemporalen Datensätzen. Aus den CSMs lässt sich die räumliche Verteilung der Pflanzenhöhen ableiten. Die Erfassung der Daten erfolgt durch Fernerkundungsmethoden aus terrestrischem Laserscanning (TLS) und Aufnahmen mit unbemannten Luftfahrzeugen (*unmanned aerial vehicles*, UAVs) in Kombination mit *computer vision*-Techniken. Die Eignung beider Methoden für die nicht-destruktive Bestimmung von Pflanzenhöhe und Biomasse sind bekannt. Die noch offene Frage ist, ob beide Methoden ähnliche Informationen erfassen und inwiefern ein Vergleich der Methoden angemessen ist. Wir gehen davon aus, dass die unterschiedlichen Sensorpositionen das resultierende CSM beeinflussen. Weiterhin nehmen wir an, dass das UAV-basierte CSM aufgrund der senkrechten Sensorposition Informationen zur Bestandsdichte enthält. Folglich erwarten wir eine niedrigere mittlere Pflanzenhöhe und größere Variation in dem UAV-basierten CSM. Die Korrelation zwischen den Pflanzenhöhen beider Methoden wurde analysiert. Ergänzend wurde eine auf einem Polygongrid basierende räumliche Analyse (zonale Statistik) zur Untersuchung des Potentials der Bestandsdichteanalyse durchgeführt. Durch diese Analyse ist es möglich, den Informationsgehalt der räumlichen Daten zu maximieren. Dafür analysierten wir frühe, mittlere und späte Entwicklungsstadien in einem Gerstenexperiment und stellten eine hohe Korrelation ($R^2 = 0.91$) zwischen den durch beide Verfahren abgeleiteten Pflanzenhöhen fest. Die aus dem UAV-Ansatz abgeleitete Pflanzenhöhe war in allen Entwicklungsstadien 0,04 m niedriger als die aus dem TLS-Ansatz abgeleitete. Allerdings war der Variationskoeffizient, entgegen der Erwartung, im TLS-Datensatz höher (4.81% Unterschied).

1 Introduction

Remote and proximal sensing technologies are of major importance in the context of precision agriculture (ATZBERGER 2013) which intends to improve nutrient, pest, and stress management to increase yield (MULLA 2013). An important crop management approach is the concept of the nitrogen nutrition index (NNI), which was introduced in the 1980s (LEMAIRE et al. 1984, Lemaire et al. 2008). The NNI is calculated by using the actual measured N content (N_{act}) and the critical N content (N_c) of a crop. N_c is the N content required for maximum biomass production from tillering up to flowering and is empirically determined based on the dry weight of above ground biomass (MISTELE & SCHMIDTHALTER 2008a). While N_c is defined for each crop from N-experiments, the determination of N_{act} can be derived by non-destructive remote or proximal spectral measurements (GREENWOOD et al. 1991, 1986). The application of the NNI for in-season crop management further requires information on dry biomass. The latter can be monitored with non-destructive sensing approaches using multi- or hyperspectral sensing, laser scanning, or optical red, green, blue (RGB) imaging (BENDIG et al. 2014, EHLERT et al. 2008, GNYP et al. 2013, HOSOI & OMASA 2009, THEN-KABAIL et al. 2000, TILLY et al. 2015).

For crop biomass monitoring, non-destructive sensor data have to be acquired according to important phenological growing stages supporting management decisions based e.g. on the before mentioned NNI. For this, the non-destructive determination of biomass is essential, because N_{act} is given in percentage of dry matter. Additionally, biomass is a key parameter for calculating the harvest index which is used for yield simulations (KEMANIAN et al. 2007). A typical approach to estimate biomass non-destructively is proximal or remote sensing (MISTELE & SCHMIDTHALTER 2008b). Besides these approaches, it is known that plant height is a strong predictor for biomass (CATCHPOLE & WHEELER 1992, FRICKE & WACHENDORF 2013). Therefore, the concept of multi-temporal Crop Surface Models (CSMs) was introduced by HOFFMEISTER et al. (2010) to derive plant height from terrestrial laser scanning (TLS) (TILLY et al. 2014). This concept of

multi-temporal CSMs was transferred to Unmanned Aerial Vehicles (UAVs) by using RGB imaging and Structure from Motion (SfM) data analysis (BENDIG et al. 2013, CRAMER et al. 2013, HAALA & ROTHERMEL 2012). Plant height from UAV-derived CSMs is also used with spectral information for yield estimation (GEIPEL et al. 2014).

CSMs can be acquired in super-high resolution (< 0.02 m) with laser scanning techniques or from UAV imagery. And it is proven for urban environments that SfM-derived Digital Surface Models (DSMs) can produce similar data quality like TLS (PERSAD & ARMENAKIS 2015, GRENZDÖRFFER et al. 2015). A study by OUÉDRAOGO et al. (2014) compared both methods for deriving DSMs of agricultural watersheds and found root-mean-square errors (RMSE) of 4.5 cm for TLS and 9.0 cm to 13.9 cm for the UAV-based DSM (fixed wing system) in a 12 ha watershed with $1\text{ m} \times 1\text{ m}$ resolution. When comparing CSMs from TLS or UAV campaigns in cropping systems, a major difference is the sensor viewing geometry. This difference should be considered due to the different canopy surface roughness of varying cropping systems. While UAV approaches capture the imagery more or less in nadir view, the TLS system has an oblique acquisition position resulting in non-homogeneous point densities (HÄMMERLE & HÖFLE 2014, EHLERT et al. 2013). Consequently, the data from the two different methods should show characteristic differences in CSM-derived plant height (PH) depending on the sensor viewing geometry and the plant density (PD). In Fig. 1 the possible effect on the CSM values is shown.

The potential differences in mean plant height values shown in Fig. 1 are a result of canopy surface roughness. Variation in plant height increases with crop surface roughness. This variation should be found in data produced from nadir viewing techniques, while oblique viewing should smooth the crop surface roughness resulting in less varying plant height values. Consequently, a hypothesis of this consideration is that nadir viewing techniques for crop surfaces are a measure of crop plant height and crop plant density within one dataset. Therefore, in this study we focus on (i) the comparison of plant height data derived

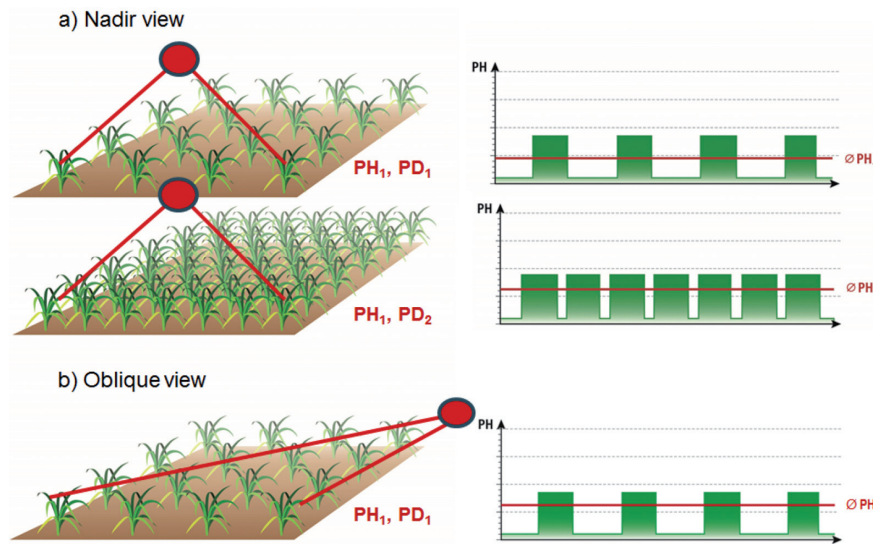


Fig. 1: The effect of different viewing geometries on the mean plant height values of crop surface models (CSMs): a) Nadir view: equal plant height (PH_1) but different plant densities (PD_1 , PD_2) result in different mean plant height values ($\bar{\text{PH}}_1 \neq \bar{\text{PH}}_2$); b) Oblique view: equal plant height (PH_1) but different plant densities (PD_1 , PD_2 (middle)) should result in similar plant height values of nadir and oblique viewing angles ($\bar{\text{PH}}_2 \approx \bar{\text{PH}}_3$). model projected with initial exterior orientation parameters, green = 3D building model projected with adjusted exterior orientation parameters.

from UAV imagery and TLS and on (ii) resampling methods keeping descriptive statistics of the plant height data as a density measure.

2 Material and Methods

2.1 Study Site and Dataset

The dataset used for the UAV and TLS comparison was partly collected within the Crop Sense.net project activity. CropSense.net was part of the German Ministry for Education and Research (BMBF) networks of excellence in agricultural and nutrition research. In this study, we used CSMs generated from the spring barley experiment site in 2013 (TILLY et al. 2015, BENDIG et al. 2014). The experiment field was situated at the Campus Klein-Altendorf agricultural research station of the Agricultural Faculty, University of Bonn, Germany ($50^{\circ}37'51''$ N, $6^{\circ}59'32''$ E, 186 m). We chose 20 preferably heterogeneous plots each $3\text{ m} \times 7\text{ m}$ (Fig. 2) for the analysis to pro-

vide sufficient difference in plant density. Although seeding density (300 plants/m^2) and row spacing (0.104 m) were identical in each plot, plant density effectively varied throughout the growing season. We analyzed data of the early (T1 = 28 May), middle (T2 = 12 June (TLS), 14 June (UAV)) and late growth stages (T3 = 10 July (TLS), 08 July (UAV)).



Fig. 2: Study site: spring barley experiment at Campus Klein-Altendorf agricultural research station; black outlines: plots, black numbers: plot numbers, background: orthophoto (28 May 2013).

2.2 Plant Height Measurements and Crop Surface Models (CSMs)

TLS and UAV data were captured preferably on the same day or at days close to each other. To ensure comparability, all data were georeferenced in the same coordinate system. Therefore, ground control points and scan positions were measured with a real-time kinematic global positioning system (RTK-GPS, HiPer® Pro by TOPCON, Tokyo, Japan). By establishing an own reference station, a relative accuracy of 0.01 m in the horizontal and vertical was achieved.

Plant height information is derived from the CSMs representing the top canopy (HOFFMEISTER et al. 2010). An additional Digital Terrain Model (DTM) needs to be established prior to plant development and serves as a ground model. CSM-derived plant height is obtained by subtracting the DTM from the CSM (BENDIG et al. 2013).

2.3 UAV

The UAV system was a MikroKopter MK-Októ (HiSystems) combined with a Panasonic Lumix GX1 digital camera (16 Megapixel, Lumix G 20 mm (F1.7 aspheric (ASPH)) fixed lens) (compare BENDIG et al. 2013, 2014). The digital camera was mounted on a gimbal in nadir position. The pitch and roll movement of the UAV are compensated by the gimbal to maintain nadir imagery. Between 342 and 783 images were captured on each date at 50 m flying height, resulting in 90% forward overlap, 60% sidelap and a ground sampling distance (GSD) of 9 mm.

The imagery was processed using the SfM technique with Agisoft PhotoScan Professional software (Szeliski 2010, SONA et al. 2014). The resulting average model point density was 2,960 points/m². 28 ground control points served as a georeference (measured with the RTK-DGPS). The resulting CSMs were further processed in Esri ArcGIS® 10 to reduce the CSMs to the plot area of interest (AOI), to exclude plot boundaries from the analysis (0.3 m on each side), and to subtract the ground model to obtain the plant height. Prior to extraction of the area of interest, the CSMs were

resampled to 10 mm raster size and smoothed using 3×3 pixel focal statistics (BENDIG et al. 2013). It was found that smoothing had no significant effect, hence this step was neglected for future data processing. The typical height accuracy of the UAV-based CSMs lies between 15 mm – 30 mm (GRENZDÖRFFER & ZACHARIAS 2014, GEIPEL et al. 2014).

2.4 TLS

The TLS device was a Riegl LMS-Z420i time-of-flight scanner with a rotating polygonal mirror allowing measurement rates of up to 11,000 points/second (RIEGL LMS GmbH 2015). A Nikon D200 digital camera (Nikon AF Nikkor 20 mm f/2.8D lens) and RTK-GPS receiver were mounted on the scanner additionally (TILLY et al. 2015).

The study site was scanned from its four corners with the scanner mounted on a hydraulic platform, resulting in a sensor height of 4 m above the ground. Ranging poles with highly-reflective cylinders were used to merge the scan positions during post processing. Registration, adjustment, merging, filtering of the point clouds, and the extraction of the area of interest were carried out in RiSCAN Pro. The different scan positions were registered by using the highly-reflective cylinders as tie points. Remaining alignment errors were corrected via multistation adjustment (a RiSCAN Pro functionality). Finally, the point clouds were reduced to the AOI and the maximum points were selected for the crop surface. The average point density after the filtering was 600 points/m² (ranging from 200–1,700 points/m²) with the point density being very heterogeneous, due to the radial measuring principle of the static position of the TLS system. Further processing was conducted in Esri ArcGIS® 10, including the interpolation of CSMs by using the inverse distance weighting (IDW) algorithm. Afterwards, the plant heights were pixel-wise calculated by subtracting a ground model from each DSM to obtain the CSMs.

2.5 Raster vs. Polygon Grids

In GIS software products, zonal statistics computes descriptive statistics (minimum, maximum, range, sum, mean, standard deviation) from a value raster file for a given set of zones in raster or vector format. The descriptive statistics are calculated for each given zone by considering all raster values within a zone.

In this study, we use polygon grids for resampling and further analysis of plant height data derived from CSMs. The polygon grid represents a raster grid which stores features in vector format. Instead of resampling the super-high resolution plant height raster data to a coarser resolution, a polygon grid in a given resolution is created and serves for zonal statistics analysis in which each single polygon grid cell serves as an individual zone.

The concept is shown in Fig. 3. The coloured raster cells represent continuous plant height data in super-high spatial resolution ($< 0.01 \text{ m}$). The black outlines represent the polygon grid in a 0.2 m resolution. Each polygon grid cell has a unique feature ID and serves as a unique zone for computing zonal statistics. The results are stored as fields in the polygon grid attribute table. In Fig. 3 the results of the zonal statistics are displayed for one polygon grid cell. The statistics are computed from the values of 1,024 raster cells.

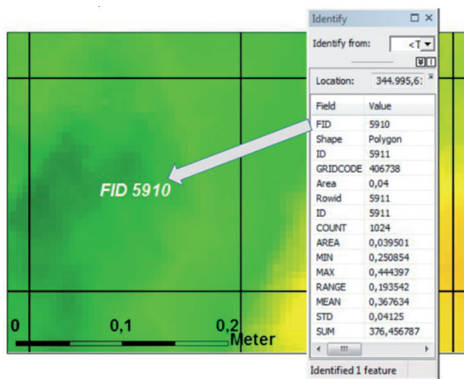


Fig. 3: Example: CSM in super-high resolution ($< 0.01 \text{ m}$) and a corresponding polygon grid in 0.2 m resolution (black polygon outlines).

Due to the above mentioned row spacing and seeding density, a 0.3 m polygon grid was produced for this study from a resampled CSM raster by converting it into a polygon vector dataset. The resulting polygon grid served as zone data for calculating the descriptive statistics. We chose the mean plant height and the coefficient of variation (CV, i.e. the ratio of standard deviation and mean) for further analysis.

3 Results

According to the objectives of the study, the results for the comparison between UAV-derived plant heights and TLS-derived plant heights are divided into a direct comparison and the polygon grid analysis.

3.1 UAV-CSM vs. TLS-CSM

The comparison of TLS- and UAV-derived plant height from corresponding CSMs is presented in Fig. 4. The data represent the averaged plant height per plot of the above described barley experiment for three dates in 2013 ($n = 60$). As hypothesized in the introduction, the UAV-derived plant height data with nadir view have lower values compared to the TLS-derived values with the oblique view. However, the differences are much smaller than expected, but, as shown in Fig. 5, in the early growing season (T1) the differences are more characteristic than in later growth stages after canopy closure (T2). The latter is due to a smoother canopy surface. In the very late growth stage (T3) the TLS data are higher but no clear trend is observed. In general, CSM-derived plant height derived from both methods is closely related resulting in a R^2 of 0.91 overall growth stages and for T1, T2, and T3, in R^2 of 0.57, 0.72, and 0.26, respectively.

3.2 Polygon Grids for CSM Analysis

For this study, a 0.3 m polygon grid was produced from a resampled CSM raster by converting it into a polygon vector dataset representing continuous raster data in vector data

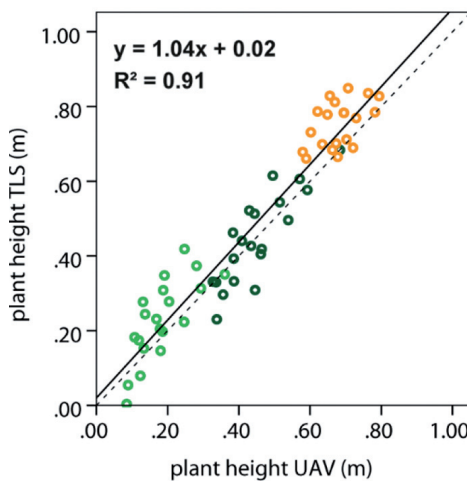


Fig. 4: Scatter plot for plant height from UAV and TLS (m) for observation dates T1 (light green), T2 (dark green), T3 (orange) ($n = 60$). Solid line = regression line, dashed line = 1:1 line, R^2 = coefficient of determination; $p < 0.0001$.

format. The resulting polygon grid serves as zone data for calculating descriptive statistics for each polygon grid cell using zonal statistics in ArcGIS®. The results for the computed mean plant height and CV are presented in Figs. 6 and 7. As already shown in Fig. 4 and hypothesized in the introduction, the mean plant heights of the UAV approach tend to be lower compared to that in the TLS approach. The difference is clearly visible in Fig. 6. Overall, the cells of the UAV polygon

grid are dominated by colours representing lower plant height values than the TLS ones in all three growth stages. But surprisingly, the plant height pattern within the plots seems to be very different between the two methods in all three growth stages.

However, the computed CV shown in Fig. 7 clearly shows that the plant height values of the UAV approach vary less compared to the TLS data in all plots and in all three growth stages. Furthermore, it is again clearly visible that the two methods show different spatial patterns within the plots. This difference in the coefficient of variation was not expected and contradicts the working hypothesis that the oblique viewing angle of the TLS produces smoother surfaces with lower variance in the plant height values.

4 Discussion and Conclusion

The focus of this study was the comparison of CSM-derived plant height in agricultural crops from terrestrial laser scanning (TLS) and unmanned aerial vehicle (UAV)-based imaging by using analyses based on polygon grids. The accuracy of both the TLS-derived and the UAV-based plant height is comparable and can be used for non-destructive determination of plant height and biomass. Our previous, multi-temporal studies showed that TLS-derived plant height explained 88–95% and UAV-based plant height explained 92% of the variation in plant height compared to manual

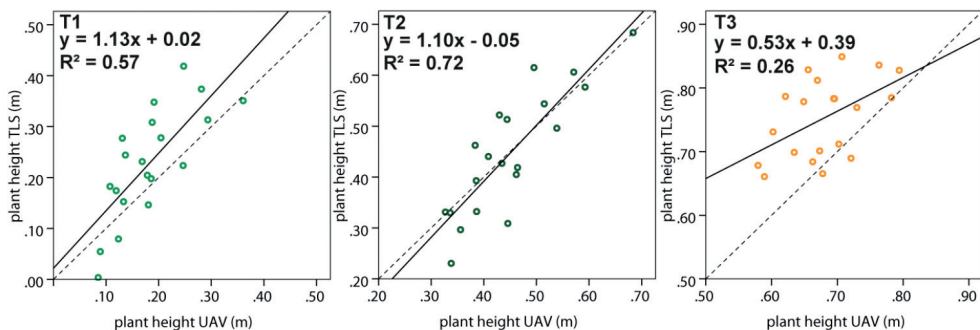


Fig. 5: Scatter plots for plant height from UAV and TLS (m) for each observation date T1, T2, and T3 ($n = 20$). Solid line = regression line, dashed line = 1:1 line, R^2 = coefficient of determination; $p < 0.0001$.

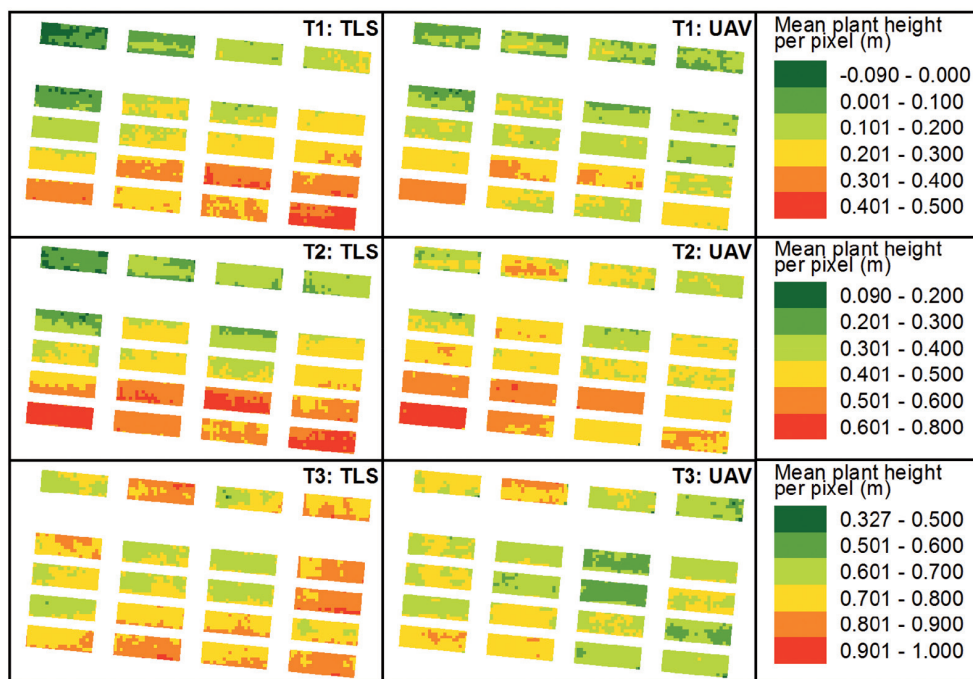


Fig. 6: Polygon grid (0.3 m pixel size) showing mean plant height per pixel for TLS and UAV.

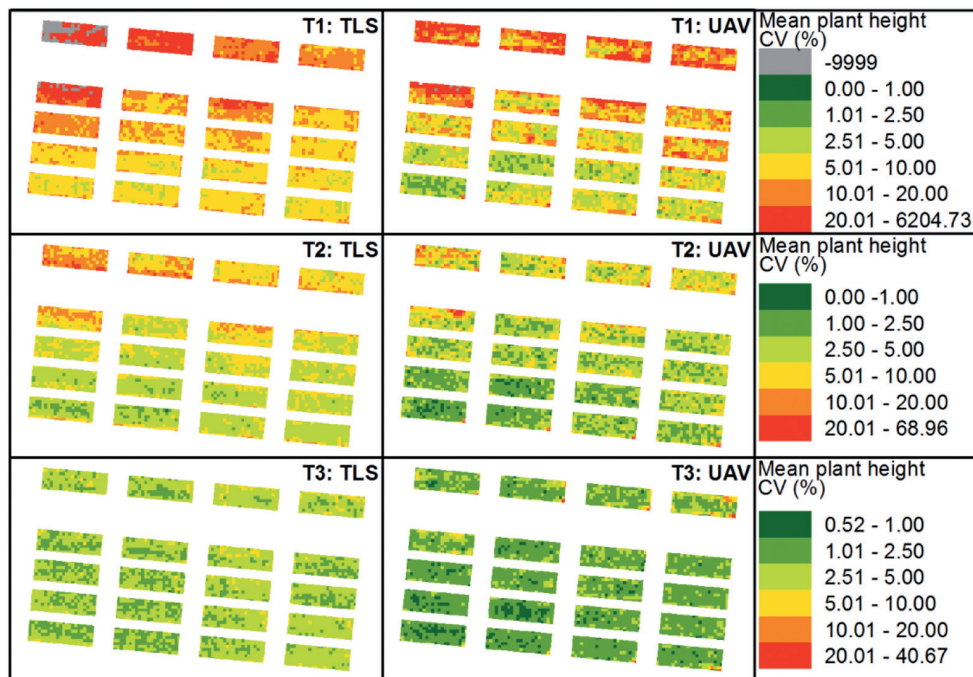


Fig. 7: Polygon grid (0.3 m pixel size) showing coefficient of variation (CV) per pixel for TLS and UAV.

measurements (TILLY et al. 2014, 2015, BENDIG et al. 2013, 2014). Furthermore, the correlation is high between the TLS- and the UAV-derived plant height in this study ($R^2 = 0.91$). However, when comparing different growth stages the correlation is lower for later growth stages. A possible explanation could be that the effect of different viewing geometries increases when canopy properties change. GRENZDÖRFFER & ZACHARIAS (2014) indicated that wind might affect measurements in senescent grains stronger and that UAV-based plant canopies contain different numbers of soil pixels in different growth stages. The same is probably true for the TLS approach but potentially does not have a similar effect due to the differing viewing geometries. Due to calm weather conditions during the field campaigns, wind most probably did not influence our analysis.

It was hypothesized that the different viewing geometries, oblique (TLS) versus nadir (UAV), result in higher variance of the UAV-derived plant height data and in lower mean plant height values. Therefore, the nadir viewing angle provides mean plant height information which includes a plant density measure. The latter was indicated by BARETH et al. (2015) for a grassland experiment where UAV-derived plant height was evaluated against rising plate meter measurements, which represent a compressed plant density-dependent height information, resulting in an R^2 of 0.89. But in our study the introduced hypotheses could not be proofed completely. While the mean plant height values indicate the expected trend for the TLS- and UAV-based crop surface models (CSMs) with the UAV-derived values being 0.04 m lower on average, the hypothesized explanation based on the higher CSM roughness could not be proofed. We expected a higher variance in the UAV data compared to the TLS data. In fact, the coefficient of variance being 4.81% higher in the TLS data showed the contrary. The data obtained from the two different methods exhibited different spatial patterns, which were not expected either, due to the high correlation between the mean plots. A reason could be the data processing of both approaches, which includes filtering and resampling. In our study, we just compared the final processed CSM-derived plant height values. Consequently,

we propose that a comparison of the original datasets, the point clouds, would be more appropriate in the future. For the latter, a key issue – and to our knowledge this was not discussed before – a new measurement protocol for the destructively measured ground truth must be developed. The traditional agronomic plant parameter measurements do not fit the accuracy of these sensing approaches. The plot-wise determination of ground truth is just not sufficient because it does not capture the spatial variability of plant height or biomass in the resolution of several cm or dm. Therefore, we propose the manual acquisition of continuous RTK-based plant-height profile measurements in the same resolution as the sensing approaches deliver. The same accounts for the biomass sampling, which must be taken from individual plant with known locations. Only with such ground truth data, the real and new potential of nadir- or oblique-derived CSMs as a plant height and plant density measure can be further investigated.

Acknowledgements

Some of the data used in this study was acquired within the CROP.SENSE.net project in context of the Ziel 2-Programm NRW 2007–2013 “Regionale Wettbewerbsfähigkeit und Beschäftigung”, financially supported by the Ministry for Innovation, Science and Research (MIWF) of the state North Rhine Westphalia (NRW) and European Union Funds for regional development (EFRE) (005-1103-0018).

References

- ATZBERGER, C., 2013: Advances in Remote Sensing of Agriculture: Context Description, Existing Operational Monitoring Systems and Major Information Needs. – *Remote Sensing* **5** (2): 949–981; doi: 10.3390/rs5020949.
- BARETH, G., BOLLEN, A., HOLLBERG, J., AASEN, H., BURKHART, A. & SCHELLBERG, J., 2015: Feasibility study of using non-calibrated UAV-based RGB imagery for grassland monitoring: Case study at the Rengen Long-term Grassland Experiment (RGE), Germany. – *DGPF Annual Conference*’**15**: 55–62, Cologne.

- BENDIG, J., BOLTEN, A. & BARETH, G., 2013: UAV-based imaging for multi-temporal, very high resolution crop surface models to monitor crop growth variability. – PFG – Photogrammetrie, Fernerkundung, Geoinformation **6**: 551–562; doi: 10.1127/1432-8364/2013/0200.
- BENDIG, J., BOLTEN, A., BENNERTZ, S., BROSCHET, J., EICHFUSS, S. & BARETH, G., 2014: Estimating biomass of barley using Crop Surface Models (CSMs) derived from UAV-Based RGB Imaging. – Remote Sensing **6** (11): 10395–10412; doi: 10.3390/rs61110395.
- CATCHPOLE, W.R. & WHEELER, C.J., 1992: Estimating plant biomass: A review of techniques. – Australian Journal of Ecology **17**: 121–131; doi: 10.1111/j.1442-9993.1992.tb00790.x.
- CRAMER, M., HAALA, N., ROTHERMEL, M., LEINNESS, B. & FRITSCH, D., 2013: UAV@LGL – Pilot Study of the Use of UAV for National Mapping in Germany. – PFG – Photogrammetrie, Fernerkundung, Geoinformation **5**: 495–509; doi: 10.1127/1432-8364/2013/0195.
- EHRLERT, D., HORN, H.-J. & ADAMEK, R., 2008: Measuring crop biomass density by laser triangulation. – Computers and Electronics in Agriculture **61**: 117–125.
- EHRLERT, D. & HEISIG, M., 2013: Sources of angle-dependent errors in terrestrial laser scanner-based crop stand measurement. – Computers and Electronics in Agriculture **93**: 10–16.
- FRICKE, T. & WACHENDORF, M., 2013: Combining ultrasonic sward height and spectral signatures to assess the biomass of legume-grass swards. – Computers and Electronics in Agriculture **99**: 236–247.
- GEIPEL, J., LINK, J. & CLAUPEIN, W., 2014: Combined spectral and spatial modeling of corn yield based on aerial images and crop surface models acquired with an unmanned aircraft system. – Remote Sensing **6**: 10335–10355.
- GNYP, M.L., YU, K., AASEN, H., YAO, Y., HUANG, S., MIAO, Y. & BARETH, G., 2013: Analysis of Crop Reflectance for Estimating Biomass in Rice Canopies at Different Phenological Stages. – PFG – Photogrammetrie, Fernerkundung, Geoinformation **4**: 351–365; doi: 10.1127/1432-8364/2013/0182.
- GREENWOOD, D.J., NEETESON, J.J. & DRAYVOTT, A., 1986: Quantitative relationships for the dependence of growth rate of arable crops on their nitrogen content, dry weight and aerial environment. – Plant and Soil **91** (3): 281–301.
- GREENWOOD, D.J., GASTAL, F., LEMAIRE, G., DRAYCOTT, A., MILLARD, P. & NEETESON, J.J., 1991: Growth Rate and % N of Field Grown Crops: Theory and Experiments. – Annals of Botany **67** (2): 181–190.
- GRENZDÖRFFER, G.J., NAUMANN, M., NIEMEYER, F. & FRANK, A., 2015: Symbiosis of UAS Photogrammetry and TLS for Surveying and 3D Modelling of Cultural Heritage Monuments – A Case Study about the Cathedral of St. Nicholas in the City of Greifswald. – ISPRS – International Archives of the Photogrammetry, Remote Sensing and Spatial Information Sciences XL-1/W4: 91–96; doi: 10.5194/isprsarchives-XL-1-W4-91-2015.
- GRENZDÖRFFER, G. & ZACHARIAS, P., 2014: Bestands-höhenermittlung landwirtschaftlicher Kulturen aus UAV-Punktwerken. – 34. Wissenschaftlich-Technische Jahrestagung der DGPF, Hamburg.
- HAALA, N. & ROTHERMEL, M., 2012: Dense Multi-Stereo Matching for High Quality Digital Elevation Models. – PFG – Photogrammetrie, Fernerkundung, Geoinformation **4**: 331–343; doi: 10.1127/1432-8364/2012/0121.
- HÄMMERLE, M. & HÖFLE, B., 2014: Effects of reduced terrestrial LiDAR point density on high-resolution grain crop surface models in precision agriculture. – Sensors **14** (12): 24212–24230; doi: 10.3390/s141224212.
- HOFFMEISTER, D., BOLTEN, A., CURDT, C., WALDHOFF, G. & BARETH, G., 2010: High-resolution Crop Surface Models (CSM) and Crop Volume Models (CVM) on field level by terrestrial laser scanning. – Guo, H. & Wang, C. (eds.): SPIE Sixth International Symposium on Digital Earth: Models, Algorithms, and Virtual Reality. – Beijing, China: 78400E–78400E6.
- HOSOI, F. & OMASA, K., 2009: Estimating vertical plant area density profile and growth parameters of a wheat canopy at different growth stages using three-dimensional portable lidar imaging. – ISPRS Journal of Photogrammetry and Remote Sensing **2** (64): 151–158.
- KEMANIAN, A.R., STÖCKLE, C.O., HUGGINS, A.R. & VIEGA, L.M., 2007: A simple method to estimate harvest index in grain crops. – Field Crops Research **103** (3): 208–216.
- LEMAIRE, G., JEUFFROY, M.-H. & GASTAL, F., 2008: Diagnosis tool for plant and crop N status in vegetative stage: Theory and practices for crop N management. – European Journal of Agronomy **28** (4): 614–624.
- LEMAIRE, G., SALETTE, J., SIGOGNE, M. & TERRASSON, J.-P., 1984: Relation entre dynamique de croissance et dynamique de prélèvement d'azote pour un peuplement de graminées fourragères. I. – Etude de l'effet du milieu. – Agronomy for Sustainable Development **4** (5): 423–430; doi: 10.1051/agro:19840503.
- MISTELE, B. & SCHMIDHALTER, U., 2008a: Estimating the nitrogen nutrition index using spectral canopy reflectance measurements. – European Journal Agronomy **29**: 184–190.

- MISTELE, B. & SCHMIDTHALTER, U., 2008b: Spectral measurements of the total aerial N and biomass dry weight in maize using a quadrilateral-view optic. – *Field Crops Research* **106** (1): 94–103.
- MULLA, D.J., 2013: Twenty five years of remote sensing in precision agriculture: key advances and remaining knowledge gaps. – *Biosystems Engineering* **114** (4): 358–371.
- PERSAD, R.A. & ARMENAKIS, C., 2015: Alignment of Point Cloud DSMs from TLS and UAV Platforms. – *ISPRS – International Archives of the Photogrammetry, Remote Sensing and Spatial Information Sciences XL-1/W4*: 369–373; doi: 10.5194/isprsarchives-XL-1-W4-369-2015.
- OUÉDRAOGO, M.M., DEGRÉ, A., DEBOUCHE, C. & LISEIN, J., 2014: The evaluation of unmanned aerial system-based photogrammetry and terrestrial laser scanning to generate DEMs of agricultural watersheds. – *Geomorphology* **214**: 339–355.
- RIEGL LMS GMBH, 2015: Datasheet Riegl LMS-Z420i. – http://www.riegl.com/uploads/tx_pxriegldownloads/10_DataSheet_Z420i_03-05-2010.pdf (1.9.2015).
- SONA, G., PINTO, L., PAGLIRAI, D., PASSONI, D. & GINI, R., 2014: Experimental analysis of different software packages for orientation and digital surface modelling from UAV images. – *Earth Science Informatics* **7**: 97–107; doi: 10.1007/s12145-013-0142-2.
- SZELISKI, R., 2010: Computer Vision: Algorithms and Applications. – 824 p., Springer, London, UK.
- THENKABAIL, P.S., SMITH, R.B. & DE PAUW, E., 2000: Hyperspectral Vegetation Indices and their relationships with agricultural crop characteristics. – *Remote Sensing Environment* **71** (2): 158–182.
- TILLY, N., HOFFMEISTER, D., CIAO, Q., HUANG, S., MIAO, Y., LENZ-WIEDEMANN, V. & BARETH, G., 2014: Multi-temporal Crop Surface Models: Accurate plant height measurement and biomass estimation with terrestrial laser scanning in paddy rice. – *Journal of Applied Remote Sensing* **8** (1): 083671-1–083671-22; doi: 10.1117/1.JRS.8.083671.
- TILLY, N., AASEN, H. & BARETH, G., 2015: Fusion of plant height and vegetation indices for the estimation of barley biomass. – *Remote Sensing* **7** (9): 11449–11480; doi: 10.3390/rs70911449.

Addresses of the Authors:

Prof. Dr. GEORG BARETH, Dr. JULIANE BENDIG, NORA TILLY, Dr. DIRK HOFFMEISTER, HELGE AASEN & Dr. ANDREAS BOLTEN, Institute of Geography, GIS & RS Group, University of Cologne, Albertus-Magnus-Platz, D-50923 Köln, Tel.: +49-221-470-6551, Fax: +49-221-470-1638, e-mails:{g.bareth}{juliane.bendig}{nora.tilly}{dirk.hoffmeister}{helge.aasen}{andreas.bolten}@uni-koeln.de

Manuskript eingereicht: Oktober 2015

Angenommen: Januar 2016

Berichte von Veranstaltungen

ISPRS Geospatial Week 2015, 28. September – 2. Oktober 2015, La Grande Motte, Frankreich

Vom 28. September bis 2. Oktober 2015 fand die ISPRS Geospatial Week 2015 in La Grande Motte, einem Ort in der Nähe von Montpellier, statt. Die Veranstaltung wurde von der Société Française de Photogrammétrie et de Télédétection (SFPT), dem Institut National de l'Information Géographique et Forestière (IGN), dem Institut National de Recherche en Sciences et Technologies pour l'Environnement et l'Agriculture (IRSTEA) und dem Office National des Forêts (ONF) organisiert. Mehr als 500 Teilnehmer aus 52 Ländern waren registriert.

Insgesamt setzte sich die ISPRS Geospatial Week 2015 aus 11 verschiedenen Workshops zusammen, welche teils sequentiell, teils parallel zueinander abgehalten wurden:

- SilviLaser
- ISPRS Workshop Laser Scanning
- CMRT - City Models, Roads and Traffic
- ISA - Image Sequence Analysis
- ISSDQ - International Symposium on Spatial Data Quality
- Gi4DM - International Conference on Geo-information for Disaster Management
- GeoBigData
- GeoUAV
- GeoHyper
- GeoVIS
- RSDI - Remote Sensing Data Infrastructures

Die einzelnen Workshops waren wiederum in Oral Sessions und Poster Sessions gegliedert. Zusätzlich wurde im Rahmen der gesamten Veranstaltung mit 19 Vorträgen von eingeladenen Gastrednern bezüglich verschiedener Themengebiete ein interessanter Überblick über den gegenwärtigen Stand der Forschung sowie aktuelle Trends gegeben. Das gesamte Vortragsprogramm war so aufeinander abgestimmt, dass zentrale eingeladene

Vorträge von allen Konferenzteilnehmern besucht werden konnten.

Wie gewohnt gab es für die Einreichung von Beiträgen wieder zwei unterschiedliche Modalitäten. Zum einen konnten vollständige Beiträge mit einem Umfang von maximal acht Seiten für eine anonyme Begutachtung eingereicht werden. Zum anderen war es möglich, Kurzfassungen von Beiträgen für eine Begutachtung einzureichen und den vollständigen Beitrag bei Annahme durch die Gutachter nachzureichen. Insgesamt wurden 344 Beiträge eingereicht, von denen 162 angenommen wurden. Von denjenigen wissenschaftlichen Beiträgen, deren Begutachtung auf dem gesamten Beitrag basierte, wurden 71 Beiträge im Band II-3/W5 der *ISPRS Annals of the Photogrammetry, Remote Sensing and Spatial Information Sciences* publiziert und auf der Internetseite der ISPRS zur Verfügung gestellt. Von den anderen, deren Begutachtung nur auf der Kurzfassung basierte, wurden 91 im Band XL-3/W3 der *International Archives of the Photogrammetry, Remote Sensing and Spatial Information Sciences* publiziert und ebenfalls auf der Internetseite der ISPRS zur Verfügung gestellt.

Zusammenfassend ist festzuhalten, dass die gesamte Veranstaltung hervorragend organisiert war, wofür den Verantwortlichen und Helfern herzlich zu danken ist. Die Vortragsblöcke waren interessant gestaltet und boten einen breiten Einblick in viele Themengebiete, ohne es dabei an der nötigen fachlichen Tiefe fehlen zu lassen. Besonders hervorzuheben sind neben dem meist ausgezeichneten fachlichen Niveau der Veranstaltung auch der sehr gelungene technische Ablauf, aber auch die bereits im Vorfeld termingerecht durchgeführte Koordinierung des Review-Prozesses sowie die Bereitstellung von Informationen auf der Internetseite. Ebenso wird das den Teilnehmern bereitgestellte Mittagessen sowie das ansprechende Ambiente während der Social Events vielen Teilnehmern sicher noch sehr lange in guter Erinnerung bleiben.

Die nächste ISPRS Geospatial Week findet voraussichtlich im September 2017 in Wuhan, China, statt.

STEFFEN URBAN und MARTIN WEINMANN,
Karlsruhe

Tagung „Alle Orte, alle Zeiten“, 4./5. November 2015, Hamburg

Die Tagung *Alle Orte, alle Zeiten – Sicherung von Geobasisdaten als Gemeinschaftsaufgabe von Archiven und Vermessungsverwaltungen* fand am 4. und 5. November 2015 im Kongresszentrum des Landesbetriebs Geoinformation und Vermessung Hamburg statt.

Begrüßt wurden die über 100 Tagungsteilnehmer aus Deutschland, der Schweiz und aus Norwegen von ROLF-WERNER WELZEL, Geschäftsführer des Landesbetriebs Geoinformation und Vermessung Hamburg, von Udo SCHÄFER, Amtsleiter des Staatsarchivs Hamburg im Namen der Konferenz der Leiterinnen und Leiter der Archivverwaltungen des Bundes und der Länder (KLA) und von ANDREAS SCHLEYER, Vorsitzender der Arbeitsgemeinschaft der Vermessungsverwaltungen der Länder der Bundesrepublik Deutschland (AdV). Alle drei Redner wiesen in ihren einführenden Worten auf die hohe Bedeutung des vorgelegten Abschlussberichtes *Leitlinien zur bundesweit einheitlichen Archivierung von Geobasisdaten* für die Archiv- und Vermessungsverwaltungen der Länder hin. Selbst die Hamburger Senatorin für Stadtentwicklung ließ ausrichten, sie „drücke die Däumen“ für eine erfolgreiche Umsetzung. Der Abschlussbericht ist das Ergebnis einer gemeinsamen Arbeitsgruppe von Vertretern der Archiv- und der Vermessungsverwaltungen der Länder.

Zur Einführung in das Thema stellte ANTON PFANNENSTEIN, Landesamt für Digitalisierung, Breitband und Vermessung Bayern, die Produkte des amtlichen deutschen Vermessungswesens vor. SANDRA REIN, Landesbetrieb Landesvermessung und Geobasisinformation Brandenburg, zeigte den Teilnehmern in einer Internetpräsentation die Präsentations- und Vertriebsmöglichkeiten der Geobasisdaten

durch die Vermessungsverwaltungen der Länder am Beispiel Brandenburgs. Sie lenkte dabei den Fokus der Zuhörer darauf, dass die Nutzer von Archiven auch zukünftig für ihre Recherchen insbesondere bei Vektordaten eine Kartenvisualisierung und Suchfunktionen zum schnellen Auffinden erwarten. Über die lange Tradition bei der Archivierung von Karten und topographischen Informationen, also einer Vorgeschichte zu den vorgelegten Leitlinien, informierte BERNHARD GRAU, Generaldirektion der Archive Bayerns, anhand von eindrucksvollen Beispielen. In diesem Zusammenhang wies er auf die Bedeutung der Karten zur Rekonstruktion historischer Entwicklungsabschnitte hin und damit auf den besonderen Wert, den Geoinformationen für die Nachwelt darstellen.

Einen inhaltlichen Überblick zum Abschlussbericht gab, in Vertretung von CHRISTIAN KILLICHES, Leiter der gemeinsamen Arbeitsgruppe, ECKHARDT SEYFERT vom Landesbetrieb Landesvermessung und Geobasisinformation Brandenburg. Er hob hervor, dass mit den Leitlinien verschiedene Aktivitäten in den Ländern nun zu einem einheitlichen Vorgehen zusammengeführt worden seien. Damit können jetzt Geobasisdaten für die Nachwelt flächendeckend in einheitlichen Zeitschnitten, Dateninhalten und Datenformaten vorgehalten werden. Weiterhin werden durch die Leitlinien für die Beteiligten Hinweise gegeben, wie mit Geobasisdaten vor der AFIS-ALKIS-ATKIS®-Einführung verfahren werden soll, welche Metadaten den Archiven bei der Übergabe der Daten von den Vermessungsverwaltungen zu übergeben sind und welche Zugangsrechte für die Geobasisdaten durch die Archive insbesondere bei personenbezogenen aber auch bei speziellen technischen Daten zu beachten sind.

Anschließend stellte JENNY KOTTE, Staatsarchiv Hamburg, das Bewertungsmodell für Geobasisdaten vor. Die Arbeitsgruppe hat Empfehlungen erarbeitet, welche Daten aus heutiger Sicht dauerhaft bei den Archiven zu erhalten sind. Sie erläuterte dabei die angehaltenen übergreifenden Kriterien und daraus abgeleitet auch Einzelkriterien, die für einen bleibenden Wert von Geobasisdaten sprechen.

Im abschließenden Vortrag des ersten Tages stellte URS GERBER, Schweizer Bundesamt

für Landestopografie (swisstopo), das Projekt „Ellipse“ vor. Der Bericht über dieses Projekt gab interessante Einblicke zu der intensiven und seit vielen Jahren praktizierten Zusammenarbeit von swisstopo mit dem Schweizerischen Bundesarchiv. Laut GERBER sei die beste Erhaltungsmaßnahme für Geodaten, sie verfügbar zu machen und zu nutzen. Ebenso interessant war das von swisstopo entwickelte erweiterte Format Extended Worldfile (EWF) in XML für Rasterdaten, das gegenüber dem Worldfile-Format vor allem das Referenz- und Koordinatensystem explizit als Metadatum ausweist.

Der zweite Tagungstag befasste sich schwerpunktmäßig mit Grundüberlegungen zur Archivierung von Geobasisdaten und mit Erfahrungen aus der Praxis bei der Übernahme solcher Datenbestände. Zu den Rechtsfragen der Nutzung von Geobasisdaten in den staatlichen Archiven referierte CHRISTOPH SCHMIDT, Landesarchiv Nordrhein-Westfalen. In allen Bundesländern kommt ein grundsätzlich ähnliches, in seinen Feinheiten aber länderspezifisch differenziertes Archivrecht zur Anwendung. SCHMIDT erläuterte dabei die Ziele und Strukturen der archivischen Zugangsregelungen, die Zugangsrechte nach den Inhalten des Archivguts und nach Nutzergruppen (Behörden, Betroffene, Dritte) differenzieren. Wegen des bereits bei den datenhalgenden Stellen öffentlichen Charakters der meisten Geobasisdaten sind diese auch im Archiv für alle Nutzer frei verfügbar. Ausgenommen hiervon sind nur personenbezogene Daten aus ALKIS® sowie einige bestimmte Teilprodukte, die aus verwaltungstechnischen Gründen besonders schützenswert sind. Diese Daten sind für Dritte erst nach Ablauf von Schutzfristen bzw. nur unter besonderen Auflagen nutzbar. In der anschließenden Diskussion wurde klargestellt, dass die „freie Verfügbarkeit“ von Geobasisdaten im Archiv in der Regel nur ein Nutzungsrecht im Lesesaal begründet. Ein Rechtsanspruch auf Reproduktionen oder eine kommerzielle Weiterverwertung besteht nicht. Die Archive machten in diesem Zusammenhang noch einmal deutlich, dass sie weder ein Interesse noch einen gesetzlichen Auftrag haben, um hinsichtlich der Verwertung von Geobasisdaten in eine ökonomische Konkurrenz mit den Kataster- und

Vermessungsbehörden zu treten. Zudem fehlen den Archiven die gebührenrechtlichen Voraussetzungen und die benötigte technische Infrastruktur, um entsprechende Services anzubieten. Gleichwohl kann es im Zweifelsfall angebracht sein, zumindest für jüngere Daten im Zuge des Archivierungsprozesses einvernehmliche Vereinbarungen darüber zu treffen, wie mit Reproduktions- und Nachverwertungswünschen von Nutzern umgegangen werden kann und soll.

Zum Umgang mit Metadaten und den empfohlenen Formaten der entsprechend den Leitlinien abzugebenden Geobasisdaten trug KAI NAUMANN, Landesarchiv Baden-Württemberg, vor. Maßgebend für die Arbeitsgruppe war die Metadatennorm ISO 19115-1, ergänzt um Angaben, die im Verlauf des Archivierungsprozesses erhoben werden müssen. Dabei verwies der Referent auf die für die Übernahme und Erschließung von Geobasisdaten besonders wichtigen Metadaten. Diese wurden unter dem Aspekt der Datenstruktur, der Übertragung der Daten, der Katalogisierung, der Nutzung und der Bestandserhaltung erläutert. In der Diskussion zum Vortrag konnten mit den Tagungsteilnehmern einige Details zu Formatfragen geklärt werden. Das Format Esri Shapefile wurde für Datenbestände, die vor der Vereinheitlichung im AAA-Schema entstanden sind, als ein zulässiger Ersatz für das bislang verwendete Format EDBS eingeschätzt. Auch die geringe Bedeutung des Formats PDF/A bei Geodaten, die aus seiner Hüllenstruktur und seiner fehlenden Georeferenzierung hervorgeht, wurde angesprochen.

Der abschließende Vortragsblock spiegelte die bereits gesammelten Erfahrungen bei der praktischen Übernahme von Geobasisdaten in Archive wider. Zur Übernahme von Orthophotos im Staatsarchiv Hamburg informierte MICHAEL TOBEGEN. CORINNA KNOBLOCH, Landesarchiv Baden-Württemberg, berichtete über eine landesweite Übernahme mit anschließender archivischer Erschließung von gescannten und georeferenzierten Flurkarten aus dem 19. Jahrhundert zusammen mit Katasterinformationen aus dem Vorgängersystem des heutigen Amtlichen Liegenschaftskatasterinformationssystems (ALKIS®). LUTZ BANNERT referierte zur Sicherung von Daten aus dem DDR-Katastersystem COLIDO in Thü-

ringen. Die beiden ersten Vorträge handelten vor allem von dem Erfordernis, die Metadaten und Primärdaten der betreffenden Objekte so umzuformen, dass sie in den digitalen Archivsystemen Informationspakete ergeben, die aus sich selbst heraus verständlich sind. Hierfür sind vielseitige Transformations-Werkzeuge für Metadaten erforderlich. Auch das Auffinden in Katalogen der staatlichen Archive und in Geodatendiensten war den Referenten ein Anliegen, das in LEO-BW für Baden-Württemberg bereits in Ansätzen realisiert worden ist. Der Vortrag von LUTZ BANNERT war Daten gewidmet, die zwar in ihrer technischen Struktur (vergleichbar mit dem Automatisierten Liegenschaftsbuch ALB) keine besonderen Hindernisse bieten, aber kraft ihres Alters eine technikhistorische Besonderheit, vor allem aber Zeugnis eines vergangenen Wirtschafts- und Gesellschaftssystems sind.

Die vorgestellten Leitlinien zur bundesweit einheitlichen Archivierung von Geobasisdaten in Form des Abschlussberichtes der gemeinsamen AdV-KLA-Arbeitsgruppe „Archivierung von Geobasisdaten“ 2014 – 2015 haben im Vorfeld der Tagung sowohl die AdV als auch die KLA befürwortend zur Kenntnis genommen und zur Anwendung in den Bundesländern empfohlen. Zum Abschluss des ersten Tages unterzeichneten die beiden Vorsitzenden ANDREAS SCHLEYER (AdV) und ROBERT KRETZSCHMAR (KLA) ein Protokoll zum Abschlussbericht und tauschten die Berichte aus. Mit diesem symbolischen Akt sollte nochmals auf die Bedeutung der Arbeit hingewiesen werden. KRETZSCHMAR hob in seinen Worten bei der Unterzeichnung das beschlossene gemeinsame Vorgehen als einen „Mei-

lenstein“ bei der Zusammenarbeit zwischen Archiv- und Vermessungsverwaltungen hervor.

Mit der Tagung „Alle Orte, alle Zeiten“ hat die Arbeit der gemeinsamen Arbeitsgruppe vorerst einen Abschluss gefunden. Die Umsetzung muss jetzt in den Ländern begonnen werden. Viele persönliche Begegnungen zwischen Geodäten und Archivaren in den Pausen lassen hoffen, dass dieser Prozess zügig vorangeht. Wesentlich ist hierbei die Sicherung einer synchronen Überlieferung, die sich bundesweit an das geplante Terminraster für die AdV-Produkte hält. Die Arbeitsgruppenmitglieder sind sich einig in der Auffassung, dass dieser Prozess zu weiteren Fragestellungen führen wird, die letztlich nach einer geräumten Zeitspanne eine Weiterführung bzw. Evaluierung der Leitlinien erforderlich machen wird. Abschließend ging der Dank aller Tagungsteilnehmer an die Organisatoren der Tagung. Stellvertretend für alle hier nicht genannten Helfer sei JENNY KOTTE genannt.

Die Präsentationsfolien der Tagung und einzelne Vortragsmanuskripte sind ab Januar 2016 auf den Internetseiten des Bundesarchivs verfügbar. Auch der Abschlussbericht der Arbeitsgruppe ist dort vorhanden: <http://www.bundesarchiv.de/fachinformationen/kla/>. Der Abschlussbericht ist ebenfalls auf der Internetseite der Vermessungsverwaltungen der Länder der Bundesrepublik Deutschland abrufbar: <http://www.adv-online.de/Veroeffentlichungen/Broschueren-und-Faltblaetter/Informationen-der-AdV/>.

KAI NAUMANN, Ludwigsburg, und
ECKHARDT SEYFERT, Potsdam

Persönliches



Nachruf auf KENNERT TORLEGÅRD (1937 – 2016)

Die Gruppe der internationalen Photogrammeter wurde durch die traurige Nachricht überrascht, dass Prof. KENNERT TORLEGÅRD plötzlich verstorben ist.

ANDERS KENNERT INGEMAR TORLEGÅRD wurde am 21. Januar 1937 in Vätlanda in Mittelschweden geboren. Nach seinem Militärdienst als Luftbildinterpret zwischen 1956 und 1957 studierte er Vermessungswesen an der Königlich Technischen Hochschule Stockholm von 1957 bis 1961. Er schloss das Studium als Diplomingenieur ab. Von 1957 bis 1967 war er Mitarbeiter von Prof. BERTIL HALLERT an der KTH, bei dem er 1967 seine Dr. Ing. Prüfung ablegte. Von 1967 bis 1974 war er Chef-Photogrammeter bei der photogrammetrischen Firma VIAK AB in Göteborg.

Nach dem Tod von HALLERT im Jahre 1971 richtete die schwedische Regierung eine Berufungskommission mit internationaler Beteiligung aus Europa ein, welche zur Berufung KENNERT TORLEGÅRDS als Nachfolger führte.

KENNERT leitete das Institut für Photogrammetrie an der KTH von 1974 bis zu seiner Emeritierung im Jahre 2001 als ordentlicher Professor. Während dieser Zeit nahm er diverse Funktionen in der Universitätsverwaltung wahr, z.B. als Dekan der Fakultät von 1987 bis 1990, im Senat der KTH von 1991 bis 1997 und als Leiter des Organisationsausschusses für die International Space University 1993 – 1995.

Das schwedische Universitätssystem erlaubte ihm allerdings nach der Emeritierung nicht, seine internationalen Aktivitäten fortzusetzen. So verbrachte er seine Zeit damit, die französische Sprache zu erlernen, klassische Musik in zwei Orchestern zu spielen und den Sommer in seinem Ferienhaus in Simrisham im Süden Schwedens zu verbringen.

Gleich nach seiner Berufung an die KTH im Jahre 1974 etablierte sich KENNERT bald als führendes Mitglied der jüngeren Generation von Photogrammetern, zunächst als schwedischer Delegierter bei der OEEPE (jetzt Euro-SDR) seit 1977. Er blieb bis 2002 in der Euro-SDR aktiv. 1976 übernahm Schweden die Technische Kommission V der Internationalen Gesellschaft für Photogrammetrie mit KENNERT als Kommissionspräsidenten. Nach dem ISPRS Kongress 1980 in Hamburg leitete KENNERT die Arbeitsgruppe für Digitale Höhenmodelle. Beim Kongress 1984 in Rio de Janeiro wurde er zum Generalsekretär der ISPRS gewählt. Daraus ergab sich eine intensive Kooperation zwischen Kongressdirektor SHUNJI MURAI, Japan, und GOTTFRIED KONECNY in Deutschland zu einer Zeit, als sich die ISPRS von ihrer euro-amerikanischen Orientierung in eine globale wissenschaftliche Gesellschaft entwickelte. Diese intensiven Kontakte führten auch zur späteren Gründung des ISPRS „White Elephant Club“ von Senioren der Photogrammetrie im Jahre 2004, mit KENNERT als Gründungsmitglied.

In der Amtszeit von KENNERT als Präsident der ISPRS wurde auch die erste ISPRS Kommission an ein afrikanisches Land vergeben: OLAYINKA ADEKOYA aus Nigerien wurde ISPRS

Kommissionspräsidentin. Als ihre Regierung ihr die Unterstützung versagte, lud KENNERT sie zu einer ISPRS Vorstandssitzung nach Stockholm ein. Er arrangierte Besprechungen an der nigerianischen Botschaft, bei der er die wissenschaftliche Tätigkeit der nigerianischen Kollegen durch den nigerianischen Staat sicheren konnte. In diesem global integrativen Sinn wirkte KENNERT auch als Vizepräsident der ISPRS von 1992 bis 1996 und in ISPRS-Ausschüssen bis 2000 weiter.

Zwischen 1964 und 2000 hatte er an mehr als 30 ISPRS Symposien, an 10 ISPRS Kongressen, an 8 FIG Kongressen und an 5 IAC Kongressen aktiv teilgenommen. Diese Aktivitäten sind in zahlreichen Publikationen fest-

gehalten. Bei der Hundertjahrfeier der ISPRS in Wien im Jahre 2010 wurde er wegen seines totalen Engagements für die ISPRS zum „Fellow“ der Gesellschaft ernannt. Er war korrespondierendes Mitglied der Deutschen Geodätischen Kommission der Bayerischen Akademie der Wissenschaften und Ehrenmitglied der britischen Gesellschaft für Photogrammetrie und Fernerkundung.

Er wird beim ISPRS Kongress 2016 in Prag eine Lücke hinterlassen, aber sein positives Engagement wird nicht vergessen werden.

GOTTFRIED KONECNY,
Hannover

Hochschulnachrichten

Karlsruher Institut für Technologie

Dissertation von Clémence Dubois

Frau Dipl.-Ing. CLÉMENCE DUBOIS wurde am 11.11.2015 an der Fakultät für Bauingenieur-, Geo- und Umweltwissenschaften des Karlsruher Instituts für Technologie (KIT) mit der Arbeit Interferometric Synthetic Aperture RADAR and Radargrammetry towards the Categorization of Building Changes zum Dr.-Ing. promoviert.

1. Referent: Prof. Dr.-Ing. habil. STEFAN HINZ, KIT
2. Referent: Prof. Dr.-Ing. UWE SÖRGEL, TU Darmstadt

Kurzfassung:

Die Änderungsdetektion im städtischen Gebiet spielt eine immer größer werdende Rolle, sei es zum Monitoring des Fortschritts bei Neubauten oder Abrissen, für stadtplanerische Zwecke oder zur Schadensanalyse auf Gebäudeebene nach einer Katastrophe. Hierfür sind satellitengestützte SAR Daten besonders geeignet, da sie zu jeder Zeit und bei jedem Wetter eingesetzt werden können. Sie

sind z.B. nach einem Erdbeben oder einem Sturm von Vorteil, da eine terrestrische Analyse durch Ortsbegehung oft nur sehr begrenzt möglich ist.

Neben der Möglichkeit einer großflächigen Aufnahme erreicht die derzeitige Generation satellitengestützter Plattformen wie z.B. TerraSAR-X, TanDEM-X und COSMO-SkyMed Auflösungen bis zu einem Meter, was die detaillierte Analyse städtischer Gebiete erleichtert. Neben Einzelbildaufnahmen bieten ihre spezifischen Konstellationen die Anwendung weiterer SAR-Techniken, die auf mehrfacher Szenenaufzeichnung beruhen, wie z.B. SAR Interferometrie (InSAR) und Radargrammetrie. Im Vergleich zur Einzelbildanalyse ermöglichen diese Methoden eine drei-dimensionale Szenenrekonstruktion, was für die Analyse städtischer Gebiete von besonderem Interesse ist. Bei InSAR wird vor allem die Phasendifferenz zwischen zwei Aufnahmen mit ähnlichem Einfallsinkel genutzt, während bei der Radargrammetrie der Amplitudenver- satz zwischen zwei Aufnahmen unterschiedlicher Einfallsinkel analysiert wird.

Ziel dieser Arbeit ist die Erforschung solcher Techniken für eine vollautomatische und

schnelle Änderungsdetektion auf Gebäudeebene. Insbesondere die Vorteile und Einschränkungen einer kombinierten Anwendung von InSAR und Radargrammetrie in einer Notsituation werden hinsichtlich Schnelligkeit, Globalität und Genauigkeit untersucht.

Zuerst wird das Potenzial von InSAR-Phasen zur Gebäudedetektion und -rekonstruktion dargelegt. Insbesondere Gebäude-Layover, die durch die spezifische Sensorgeometrie entstehen, werden analysiert. Ihr besonderes Erscheinungsbild im interferometrischen Phasenbild ermöglicht die Entwicklung zweier unterschiedlicher Detektoren, deren kombinierte Verwendung zur Segmentierung von Gebäudehypothesen untersucht wird. Da zum Teil mehr als eine Fassade für ein bestimmtes Gebäude erkennbar ist, wird zusätzlich eine Methode zur Differenzierung angrenzender Fassaden vorgestellt. Basierend auf den extrahierten Fassadensegmenten wird ein Algorithmus entwickelt, der ihre Rekonstruktion in bekannte geometrische Formen durchführt, von denen wiederum Gebäudeparameter abgeleitet werden können.

Darüber hinaus wird die Eignung radargrammetrischer Daten für die Gebäuderekonstruktion und Änderungsdetektion auf Gebäudeebene analysiert. Hierfür erfolgt eine Fusion zwischen interferometrischem und radargrammetrischem Datensätzen, mit dem Ziel der Identifikation von Gebäudekorrespondenzen zwischen den Datensätzen und der Übertragung der Gebäudeparameter zur Verbesserung der Robustheit der radargrammetrischen Methode sowie der späteren Veränderungs-

analyse. Der entwickelte radargrammetrische Ansatz beabsichtigt die Erhaltung linearer Strukturen, die an Gebäuden gefunden werden. Folglich werden übliche Bildmatching-Verfahren modifiziert und ihr Beitrag analysiert. Das resultierende Erscheinungsbild von Gebäuden im radargrammetrischen Versatzbild wird interpretiert, was zur Erkennung spezifischer geometrischer Formen führt. Die Berücksichtigung von statistischer Information und abgeleiteten Matching-Parametern ermöglicht die Extraktion dieser Formen und die darauffolgende Ermittlung der Gebäudeparameter.

Basierend auf den durch beide Techniken extrahierten Gebäudeparametern wird ein Ansatz zur Änderungsdetektion entwickelt, der nicht nur die einfache Detektion von Veränderungen anstrebt, sondern auch deren Art und Umfang beschreibt. Hierfür werden mehrere Veränderungsklassen und -parameter eingeführt und ihre Relevanz untersucht.

In dieser Arbeit beschränkt sich die Analyse auf freistehende, rechteckige Gebäude mit einem Flachdach, die eine mittlere Höhe von ungefähr zehn Stockwerken aufweisen und sich vermehrt in Vororten von Großstädten befinden. Die Effizienz der vorgestellten Methodik wird quantitativ und qualitativ für sehr hochaufgelöste TerraSAR-X und TanDEM-X Daten an einer Großbaustelle im Nordosten von Paris bewertet.

Die Dissertation ist im Verzeichnis der Bibliothek des Karlsruher Institut für Technologie online verfügbar.

Neuerscheinung

BILL, R. (Hrsg.) 2016: *Grundlagen der Geoinformationssysteme*. 6., völlig neu bearbeitete und erweiterte Auflage. Wichmann-Verlag, 855 Seiten. ISBN 978-3-87907-607-9.

Seit über 25 Jahren zeichnet sich das Lehrbuch durch seine interdisziplinäre und internationale Betrachtungsweise aus. Der Inhalt wird durch eine Vielzahl von Abbildungen visuell unterstützt. Zahlreiche Beispiele und

Aufgaben mit Lösungen ermöglichen die eigenständige Umsetzung des Stoffes, wodurch sich dieses Werk auch ideal zum Selbststudium eignet. Die 6. Auflage wurde komplett überarbeitet und aktualisiert, völlig neue Themen wurden aufgenommen, so z.B. die durchgängige Integration des Themas Zeit als vierte Dimension von Geoinformationssystemen.

Veranstaltungskalender

2016

20. – 22. April: **Interexpo Geo-Siberia 2016 in Novosibirsk, Russland.** http://expo-geo.ru/event/4-Interekspo_GEO-SIBIR

9. – 13. Mai: **Living Planet Symposium 2016 in Prag**, Tschechien. lps16.esa.int

10. – 11. Mai: **Internationales 3D-Forum Lindau 2016 in Lindau.** 3d-forum.li

6. – 9. Juni: **EUSAR 2016 – 11th European Conference on Synthetic Aperture Radar in Hamburg.** eusar.de

7. – 9. Juni: **DGPF-OVG-SGPF Jahrestagung in Bern**, Schweiz. dgpf.de/con/jt2016.html

14. – 16. Juni: **geoinfo.potsdam.2016 – 64. Kartographentag und Geoinformatik 2016 in Potsdam.** geoinfo.dgfk.net

26. Juni – 1. Juli: **CVPR 2016 – International Conference on Computer Vision and Pattern Recognition 2016 in Las Vegas, USA.** pamitc.org/cvpr16

10. – 15. Juli: **IGARSS 2016 – International Geoscience and Remote Sensing Symposium 2016 in Peking, China.** igarss2016.org

12. – 19. Juli: **ISPRS Congress 2016 in Prag, Tschechien.** www.isprs2016-prague.com

14. – 16. September: **GEOBIA 2016 in Enschede**, Niederlande. geobia2016.com

22. – 23. September: **2nd Virtual Geoscience Conference (VGC 2016) in Bergen**, Norwegen. virtualoutcrop.com/vgc2016

25. – 28. September: **ICIP 2016 – International Conference on Image Processing 2016 in Phoenix**, USA. ieeicip2016.org

10. – 16. Oktober: **ECCV 2016 – European Conference on Computer Vision 2016 in Amsterdam**, Niederlande. eccv2016.org

11. – 13. Oktober: **Intergeo 2016 in Hamburg**, Deutschland. intergeo.de

8. – 11. November: **ICPR 2016 – International Conference on Pattern Recognition 2016 in Cancun**, Mexiko. icpr2016.org

Weitere Konferenzen und Workshops finden sich beispielsweise unter:
isprs.org/calendar/Default.aspx
conferences.visionbib.com

Korporative Mitglieder

Firmen

AEROWEST GmbH
 AICON 3D Systems GmbH
 aphos Leipzig AG
 ASTEC GEODATA GmbH
 Bernhard Harzer Verlag GmbH
 Black Bridge AG
 Blom Deutschland GmbH
 Brockmann Consult GmbH
 bsf swissphoto GmbH
 Büro Immekus
 DB Netz AG
 DELPHI IMM GmbH
 Deutsches Bergbau-Museum
 EFTAS Fernerkundung Technologietransfer GmbH
 ESG Elektroniksystem- und Logistik-GmbH
 Esri Deutschland GmbH
 EUROPEAN SPACE IMAGING
 Eurosense GmbH
 Exelis Visual Information Solutions GmbH
 fokus GmbH
 GAF GmbH
 GeoCart Herten GmbH
 Geoinform. & Photogr. Engin. Dr. Kruck & Co. GbR
 geopolana Ingenieurgesellschaft mbH
 GEOSYSTEMS GmbH
 GGS - Büro für Geotechnik, Geoinformatik, Service
 Hansa Luftbild AG
 Herbert Wichmann, VDE Verlag GmbH
 IAGB mbH
 IGI - Ingenieur-Gesellschaft für Interfaces mbH
 ILV-Fernerkundungs GmbH
 Infoterra GmbH
 INVERS - Industrievermessung & Systeme
 Leica Geosystems GmbH
 Linsinger ZT GmbH
 Luftbilddatenbank Dr. Carls GmbH
 map/x/tek
 Messbildstelle GmbH
 Microsoft Photogrammetry
 MILAN Geoservice GmbH
 M.O.S.S. Computer Grafik Systeme GmbH
 PHOENICS GmbH
 PMS - Photo Mess Systeme AG
 RIEGL Laser Measurement Systems GmbH
 RWE Power AG, Geobasisdaten/Markscheidewesen
 technet GmbH
 Terra-Messflug GmbH
 topometric GmbH
 TRIGIS GmbH
 Trimble Germany GmbH
 trimetric 3D Service GmbH
 Z/I Imaging Ltd.

Behörden

Bayerische Landesanstalt für Wald und Forstwirtschaft
 Bundesamt für Kartographie und Geodäsie
 Bundesministerium für Ernährung, Landwirtschaft und Verbraucherschutz
 Hessisches LA für Bodenmanagement und Geoinformation
 Innenministerium NRW, Gruppe Vermessungswesen
 Institut für Umwelt- und Zukunftsforschung
 LA für Geoinformation und Landentwicklung, BW
 LA für Vermessung und Geoinformation, Bayern

LA für Vermessung und Geoinformation, Schleswig-Holstein
 LB Geoinformation und Vermessung, Hamburg
 LB für Küstenschutz, Nationalpark und Meeresschutz, SH
 Landeshauptstadt Düsseldorf, Vermessungs- und Liegenschaftsamt
 Landesvermessung und Geobasisinformation Niedersachsen
 Märkischer Kreis, Vermessungs- und Katasteramt
 Regierungspräsident Tübingen, Abt. 8 Forstdirektion
 Regionalverband Ruhr
 Staatsbetrieb Sachsenforst
 Stadt Köln, Amt für Liegenschaften, Vermessung und Kataster
 Stadt Wuppertal, Vermessung, Katasteramt und Geodaten
 Thüringer LA für Vermessung und Geoinformation
 Zentrum für Geoinformationswesen der Bundeswehr

Hochschulen

BTU Cottbus, Lehrstuhl für Vermessungskunde
 FH Frankfurt a.M., FB 1, Studiengang Geoinformation
 FH Mainz, Institut für Raumbezogene Informations- und Messtechnik
 HCU HafenCity Universität Hamburg, Geomatik
 HfT Stuttgart, Vermessung und Geoinformatik
 HS Bochum, FB Vermessung und Geoinformatik
 HS Karlsruhe, Fakultät für Geomatik
 HTW Dresden, FB Vermessungswesen/Kartographie
 Jade Hochschule, Institut für Angewandte Photogrammetrie und Geoinformatik
 LUH Hannover, Institut für Kartographie und Geoinformatik
 LUH Hannover, Institut für Photogrammetrie und Geoinformation
 MLU Halle, FG Geofernerkundung
 Rhein Ahr Campus, Anwendungszentrum für multimediale und luftgestützte Sensorik
 Ruhr-Uni Bochum, Geographisches Institut
 RWTH Aachen, Geodätisches Institut
 TU Bergakademie Freiberg, Institut für Markscheidewesen und Geodäsie
 TU Berlin, Computer Vision & Remote Sensing
 TU Berlin, Institut für Geodäsie und Geoinformationstechnik
 TU Braunschweig, Institut für Geodäsie und Photogrammetrie
 TU Clausthal, Institut für Geotechnik und Markscheidewesen
 TU Darmstadt, Institut für Geodäsie, FG Fernerkundung und Bildanalyse
 TU Dresden, Institut für Photogrammetrie und Fernerkundung
 TU München, FG Photogrammetrie und Fernerkundung
 TU München, Lehrstuhl für Geoinformatik
 TU Wien, FG Photogrammetrie und Fernerkundung
 Uni Bonn, Institut für Photogrammetrie
 Uni Göttingen, Abt. Waldinventur und Fernerkundung
 Uni Heidelberg, IWR Interdisziplinäres Zentrum für Wissenschaftliches Rechnen
 Uni Kassel, FG Grünlandwissenschaften und Rohstoffe
 Uni Kiel, Geographisches Institut
 Uni Stuttgart, Institut für Photogrammetrie
 Uni Trier, Institut für Umweltfernerkundung und Geoinformatik
 Uni Würzburg, Geographisches Institut
 Uni zu Köln, Geographisches Institut

